ISSN 2718-322X (Online)
ISSN 1331-7210 (Print)

Engineering Power

BULLETIN OF THE CROATIAN ACADEMY OF ENGINEERING Vol. 16(3) 2021

EDITOR-IN-CHIEF'S WORD

Dear readers,

Within the scope of its task the Croatian Academy of Engineering strives to promote, explain and support the development of rapidly evolving technologies that are changing lives around the world, whatever that means.

Our distinguished member, Professor Emer. Nedjeljko Perić, Ph.D. is very involved scientifically and institutionally in projects that contribute to these changes, and we have tried to give him space in our bulletin to show us some of his achievements as well as of his associates that will surely interest you.

Editor
Vladimir Andročec, President of the Croatian Academy of Engineering

EDITOR'S WORD

Dear readers,

As an academy of engineering sciences, Croatian Academy of Engineering is specially pleased to report on collaborative research efforts between academic institutions and the industrial sector. Along this vein, in this issue of Engineering Power we present the research activities of the Laboratory for Renewable Energy Systems, Faculty of Electrical Engineering and Computing, University of Zagreb, and Innovation Centre Nikola Tesla, Zagreb, in different fields of industrial applications.

Guest-Editor is Professor Emeritus Nedjeljko Perić, Innovation Centre Nikola Tesla, and University of Zagreb, Faculty of Electrical Engineering and Computing, and Full Member of the Academy.

Editor
Zdravko Terze, Vice-President of the Croatian Academy of Engineering

FOREWORD

The Laboratory for Renewable Energy Systems (LARES) of University of Zagreb Faculty of Electrical Engineering and Computing (FER) conducts research and development of control systems based on advanced methods and digital technologies such as model predictive control and artificial intelligence methods. There is a wide range of applications that LARES deals with. To name just a few: renewable energy sources - predominantly wind and solar energy, energy storage - predominantly battery and hydrogen, complex automation in buildings, smart cities especially public lighting management, water supply management, optimization in railway transport systems. In the last two years, LARES has launched research and development projects aimed at digitization in the agri-food sector. More detailed information on ongoing and finished projects can be found at https://www.lares.fer.hr. In cooperation with the Innovation Centre Nikola Tesla (ICENT), LARES is very successful in building a network of cooperation with our and foreign companies. Construction of LARES began in 2007 based on a previously well-designed and long-term sustainable program. Today, LARES, as an integral part of the Department of Control and Computer Engineering of FER, consists of a research team of over 45 members, who are doctoral students, postdoctoral students, assistants and professors with international expertise and reputation. The author of this foreword has the honor to point out that the current head of LARES is Professor Mario Vašak who with his energy, enthusiasm, knowledge and dedication undoubtedly ensures the further very successful development of the laboratory to his satisfaction and the satisfaction of all members of the laboratory. In this issue of Engineering Power, six papers have been selected for publication. The first paper presents the original concept of the modular hierarchical model predictive control for coordinated and holistic energy management of buildings, which provides a significant reduction in the overall building operation cost. The second paper describes a case study of a real power distribution grid in Croatia focused on its dynamic reconfiguration, showing that the developed control algorithm can contribute to significant savings for the grid operator. The third paper presents the off-line and on-line optimization of the behavior of a battery system in a building for demand response provision, showing that the battery energy storage system can reduce the operating costs of a prosumer and that it can contribute to an overall electrical grid stability according to a demand response scheme. Optimal parameterization of a PV and a battery system add-on for a consumer is the fourth paper describing a procedure used for optimal sizing of the investment in a renewable electricity source and electricity storage. The fifth paper describes a case study for Croatian Railways based on coordinated energy management of the electric railway traction system. The developed algorithm is verified on a detailed real case study scenario with the presented results showing significant cost and energy consumption reductions. The sixth paper deals with the rapid plant development modelling system for predictive agriculture. Current and upcoming climate changes will evidently have the greatest impact on the cultivation of agricultural crops. Having it in mind, the paper focuses on a system concept to gather data for future models to be used publicly and interactively via a portal for predicting plant development under real and hypothetical climate conditions.

Guest-Editor
Nedjeljko Perić, Innovation Centre Nikola Tesla, and University of Zagreb, Faculty of Electrical Engineering and Computing

CONTENT

Anita Banjac[1], Nikola Hure[1], Marko Kovačević[1], Hrvoje Novak[1, 2], Mario Vašak[1], Nedjeljko Perić[2]

Modular Hierarchical Model Predictive Control for Coordinated and Holistic Energy Management of Buildings – Battery Storage Considerations

[1] University of Zagreb, Faculty of Electrical Engineering and Computing, Department of Control and Computer Engineering, Laboratory for Renewable Energy Systems, Unska 3, 10000 Zagreb, Croatia,
[2] Innovation Centre Nikola Tesla, Unska 3, 10000 Zagreb, Croatia

Abstract

In the paper, a modular building energy management strategy based on a three-level hierarchical model predictive control is applied to the daily operation scheduling of a full-scale building consisting of 248 offices. Such an approach provides a holistic energy management strategy and enables significant demand response ancillary services for buildings as prosumers, while retaining the independence of required expertise in very different building subsystems. The three-level coordination encompasses building zones, central medium conditioning and a microgrid subsystem. Compared to rule-based control, detailed realistic simulations for typical days in summer show that the indoor comfort is substantially improved with a considerable reduction of the overall building operation cost. The analysis also considers the margin of a battery storage system contribution to the operating costs reduction which underlines the potential of software-based coordination.

Keywords: *building energy management system, zone comfort control, thermal medium conditioning, microgrid energy management, hierarchical coordination, model predictive control, energy efficiency, price-optimal control*

1. Introduction

Due to the proven flexibility, a model predictive control (MPC) approach emerged as a promising solution for widespread problems of energy management within buildings. In addition to climate control, the MPC approach increases savings by 13% when applied to heat pump [1], with load shifting by up to 61% [2, 3, 4] and for peak electricity power reduction by 35-72% [5]. The introduction of microgrid in buildings enables additional savings by providing ancillary services to the utility grid or through coordinated microgrid and building climate control [6, 7].

Buildings are complex systems composed of many coupled subsystems responsible for maintaining safe and steady operation such as: building zones, central heating, ventilation and air conditioning (HVAC) system, microgrid with energy production units, storages and controllable or passive loads, etc. These subsystems differ in their dynamics, priorities, and their means of operation but also in their implementation aspects such as energy levels, protocols, maintenance services, etc. Typical applications of a building energy management system (BEMS) are only locally focused on a specific subsystem, while neglecting the interconnections and cooperation among all constituent subsystems. As a result, the building achieves uncoordinated and non-optimal behaviour. The aim of the modular building energy management strategy introduced in [6, 7] is to separate building subsystems in a hierarchical fashion rather than having one large control structure to handle all the subsystems at once. The considered BEMS consists of three levels following the building energy system vertical decomposition in its major parts: (A)

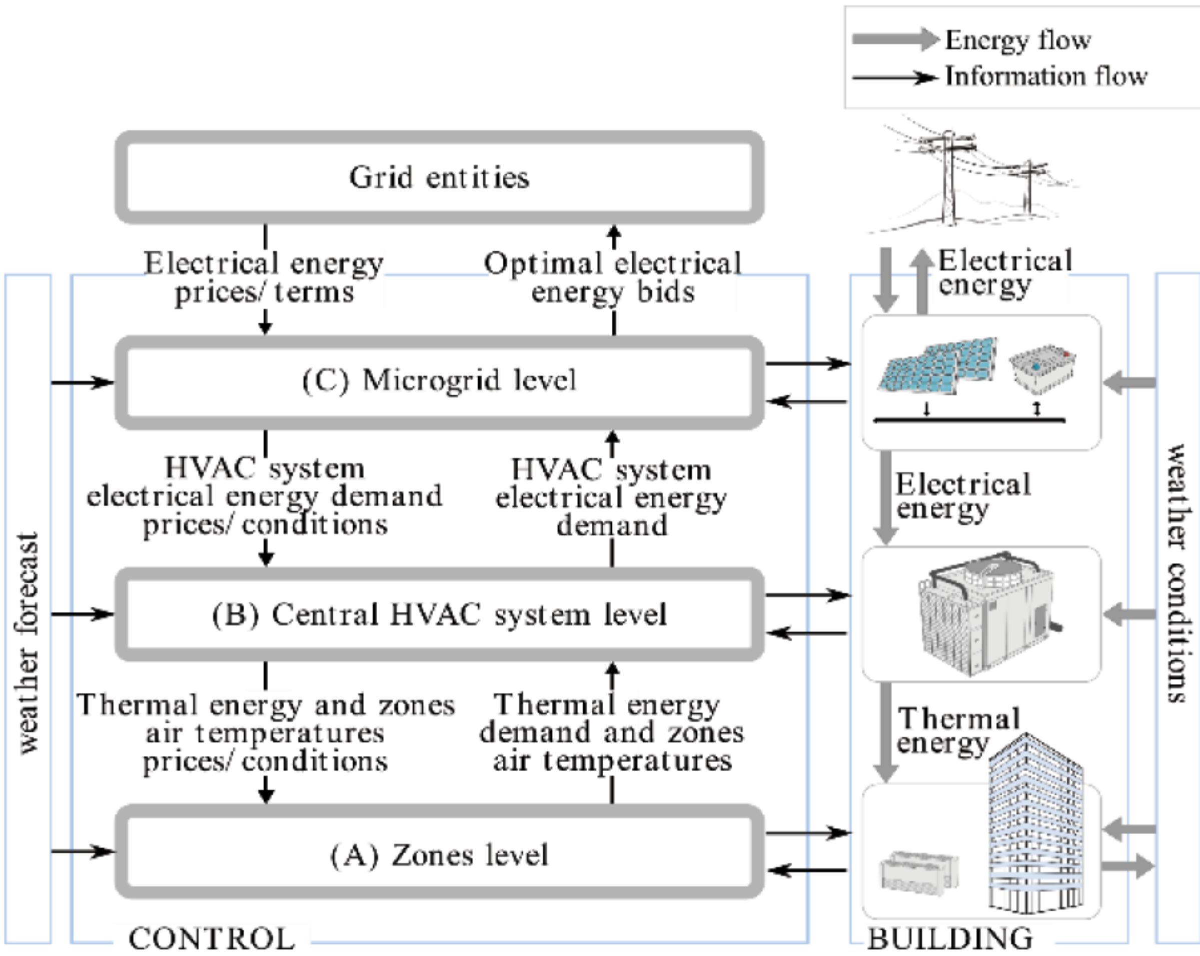

Figure 1. The modular decomposition and hierarchical coordination in a building [6, 7].

building zones level, (B) central heating/cooling medium conditioning system level (referred to as central HVAC level), and (C) building microgrid level (Fig. 1).

Zone level comfort control is envisioned as the lowest level in the proposed hierarchy. If other levels are missing, the improvement of energy-efficiency and comfort is achievable even through the application of only level (A) modules, if they consider weather forecast and comfort requirements to decide on the optimal profile of energy consumption for maintaining comfort conditions in each zone. If no other building level is present, energy prices from the utility grids are directly transferred to level (A) which then induces energy-cost-optimal behaviour instead of the energy-optimal behaviour for maintaining comfort. By also including level (B) next to level (A) the benefits can be multiplied since conventional solutions only introduce energy-connections with the central HVAC system, which consequently cannot consider the current and near-future energy requirements in the zones, and thus operates with a reduced efficiency. Especially important is the ability to intelligently shift the power demand based on the smart grid signals or predicted outdoor temperature that affects the efficiency of the central HVAC system. Finally, at level (C), the BEMS offers the possibility to manage energy storages, energy conversion systems and controllable loads at the building level. Hence, minimum energy costs can be achieved with respect to the planned energy consumption and production profile by making the building an active entity in smart grids or smart energy distribution systems at the district level. Consequently, level (C) enables further modular build-up of the concept beyond the building area and towards smart districts, grids, and cities.

The coordination in the imposed modular structure is based on the so-called "price-consumption" talk, where at each level the information about own optimal operation is communicated to the higher-level module and the cost sensitivity with respect to the lower-level operation is communicated to the lower-level module. Cost sensitivity calculation resides on multi-parametric programming and critical regions [8].

In this paper the approach developed and proposed in [6, 7] is applied to the daily operation scheduling of a full-scale skyscraper building. The benefits of the approach are demonstrated by comparing the operational costs of the building controlled by conventional control algorithms with the costs incurred by energy-optimal hierarchical building control and price-optimal coordinated building control. A special attention is put on comparing the benefits of optimal coordination achievable with and without the battery storage system.

2. Case-study analysis

The case-study building consists of 248 controllable zones equipped with two-pipe fan coil units (FCUs) for seasonal heating or cooling. The cooling energy for the building is supplied from the chiller station with the ability to control the supply temperature of the cooling medium at the central HVAC level. Besides the controllable building zones, the chiller also supplies thermal energy to the adjacent faculty building whose thermal energy consumption is considered non-controllable. The considered microgrid consists of a battery storage system with a fully controllable power converter and a solar power plant. The central HVAC level electrical energy consumption is a controllable load at the microgrid level. It consists of the consumption of the chiller and of the FCUs' fans. The non-controllable electrical energy load at the microgrid level includes the production of the solar power plant and the consumption of the office lighting, computers, building elevators as well as electrical air conditioning units in the server rooms.

2.1. Simulation scenario

The considered control strategies are validated for a typical sunny workday in July [7]. The non-controllable consumptions at the central HVAC system level and the microgrid level are estimated based on the historical building data [7]. Equivalent heat disturbances in all zones are assumed to be zero. The volatile energy market electricity prices, shown in Fig. 2, are taken from the European Power Exchange company portal [9] and scaled to match the two-tariff prices comprising grid fees and the cost of energy supplied in Croatia.

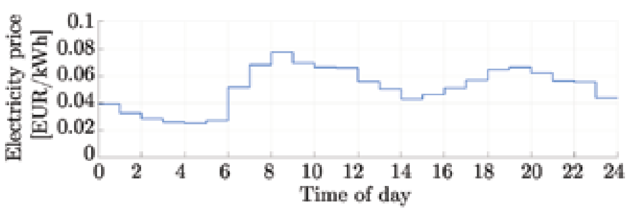

Figure 2. Day-ahead electricity price profile for grid-building energy exchange.

It is assumed that the building is occupied from 7:00 until 20:00. During the occupancy periods the zone temperature should be within an interval of 24±1.5°C. Outside that interval the allowed deviation from the temperature reference is matched with the building protect limits defined as 24±8°C.

The following control strategies are considered:

Baseline control: The baseline algorithms correspond to the usual way of commercial BEMS operation: simple discrete hysteresis control of zone temperature, supply medium temperature kept at constant predefined value, and simple transactive battery storage controller used to flatten the energy exchange profile.

Energy-optimal control: In energy-optimal control, the BEMS operates in an uncoordinated manner where each building optimization level operates independently (local-wise optimal) with only energy demands exchanged between the levels. During this exchange no feedback is provided from the superior levels regarding the consumption profiles and the corresponding energy prices and no tuning of the initial energy demands is performed.

Price-optimal control: In coordinated control, all control levels considered are joined together by the iterative parametric hierarchical coordination presented in [6, 7].

The performance of all considered control strategies is verified in a scenario with the enforced repeated behaviour from day to day, i.e. the initial state of the building (at the beginning of the day, at midnight), which is subject to optimization, is equal to the final state of the building (at the next midnight). In this way the system does not exploit any initial condition in the building to achieve savings, but leaves the building in the same condition as it was at the beginning of the day – i.e. no energy accumulated in the initial state is exploited.

All MPC controllers operate with a sampling time of 15 min. The zone level MPC equally weights the comfort and energy consumption/cost – the comfort-savings trade-off parameter [7] is set to 1. The detailed list of the considered simulation scenario parameters can be found in [7]. To review the energy flexibility and the potential of the battery energy storage, the battery degradation cost approximated to be as high as 0.226 EUR/kWh [7] is set to zero in the simulation scenario considered since for the estimated price the battery use would be completely prohibited in the case of price-optimal control. The responses of the thermal and electrical power profiles are averaged over 15-minute time intervals in all results.

2.2. Results

To fully investigate the contributions and savings possibilities of hierarchical coordination between energy flows and consumption levels, the corresponding building operation costs and achieved thermal comfort are investigated for cases with and without the battery storage system. In the case without battery storage flexibility is only achieved by modifying the central

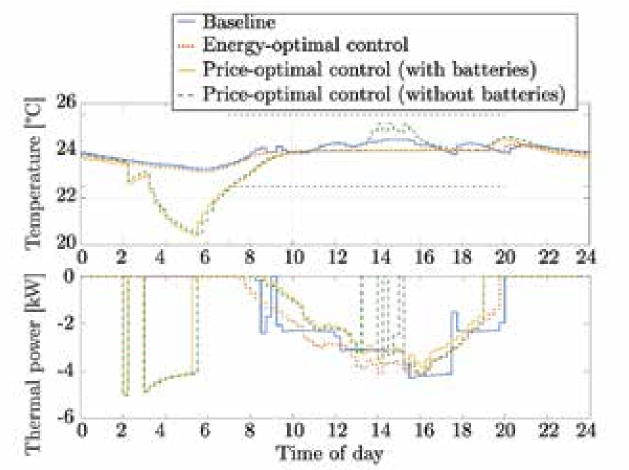

Figure 3. The temperature and mean thermal power provided from the FCUs to the zone air within the analysed day.

HVAC system consumption according to the thermal comfort demands of the building zones. The introduction of the non-wearable battery energy storage system into the building additionally increases the building flexibility and enables additional extensions of the savings margin.

Typical temperature profiles and mean thermal power provided from the FCUs to the zone air for one exemplary building zone is presented in Fig. 3

The permissible zone temperature interval during occupancy periods is shown with black dashed lines. The deviation of the zone temperature from the reference for the price-optimal control and the case without batteries in intervals around 14:00 is a clear result of coordination where the microgrid and central HVAC level force the zones to lower the thermal energy demand in intervals in which the peak power demand occurs. For the price-optimal control and the case with batteries, the peak is already flattened in the initial microgrid iteration where in all subsequent iterations the zone level thermal energy consumption is shifted towards the intervals with more beneficial electrical energy prices and HVAC system efficiency.

In the considered case of seasonal cooling, the comfort with the baseline controller is significantly disrupted in zones in which the available thermal power is insufficient to cover the peak demand. The comfort levels calculated separately for zones oriented towards north and towards south, for cases with and without batteries, are shown in Fig. 4 and compared to the resulting thermal energy consumption of the zones considered.

The comfort level indicator is measured as the average deviation from the temperature reference. The large overheating of the south-oriented zones when using the baseline control strategy is a clear result of lacking predictive feature. In both MPC based strategies the temperature in all building zones is kept within the permissible temperature range, reducing thus the overheating by up to 56% and improving the overall comfort in all building zones by at least 57%.

The energy exchange of the battery storage system and its state of energy levels during the day are depicted in Fig. 5.

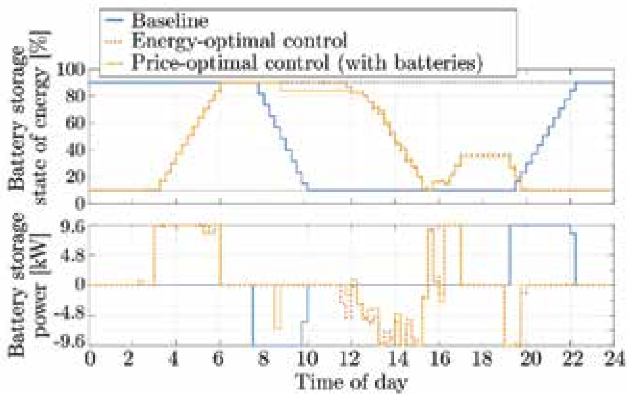

Figure 5. Battery storage state of energy and power exchange profiles.

In the MPC strategies, the batteries are charged during the lowest electricity prices in the early morning and exploited during the period 11:00-16:00 for peak power reduction. Additional savings are obtained by utilizing

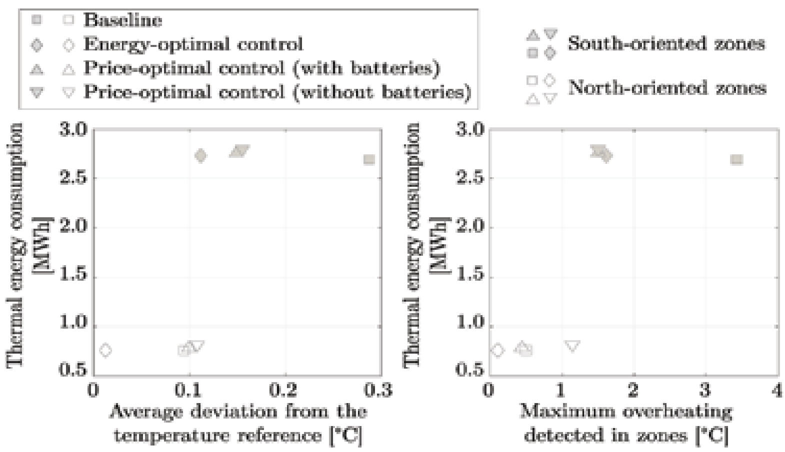

Figure 4. Comfort level indicators for different controller strategies.

the electricity price difference during the period from 16:00-20:00, when the overall building consumption is lower and a peak power reduction is not needed. Figure 5 shows that the storage system operational limits as well as operation repeatability are respected. The daily energy exchange with the distribution grid is depicted in Fig. 6.

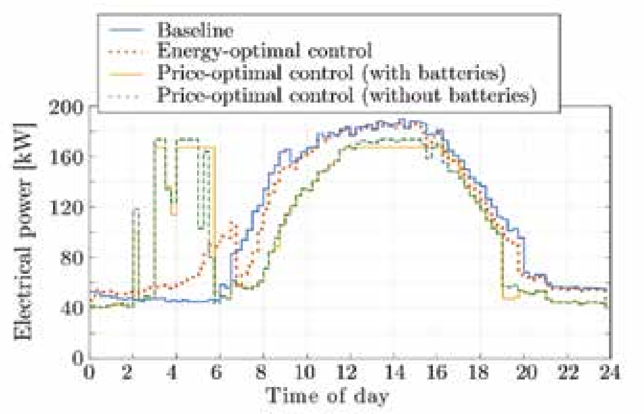

Figure 6. The overall day-ahead building energy consumption profile.

Lower electricity prices during the early morning hours from 03:00 to 06:00 are aimed to increase the overall building consumption such that the energy consumption during peak prices from 07:00 to 10:00 is decreased and the overall operation costs reduced. Additionally, the building operation costs are further reduced since the peak power consumption is decreased from 189.67 kW in the baseline scenario to 173.62 kW in the price-optimal scenario without batteries and additionally to 167.32 kW in the price-optimal scenario with batteries.

The comparison of the overall building operation costs stemming from baseline operation with the costs results obtained via energy-optimal control and price-optimal control is shown in Fig. 7.

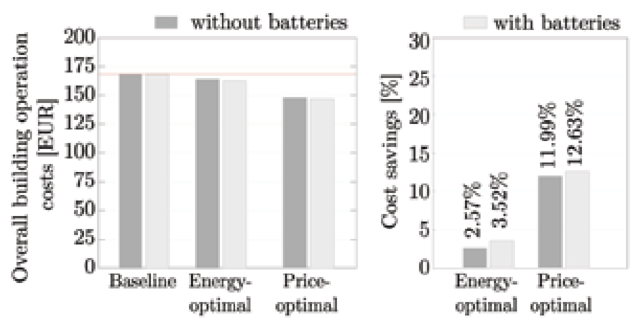

Figure 7. Comparison of overall building operation costs.

3. Conclusion

In this paper, the multi-level hierarchical model predictive control is applied to the daily operation scheduling of a full-scale skyscraper building. Coordination of the control levels of comfort in zones, heating/cooling medium preparation and building microgrid is achieved for attaining minimum building operation costs while maintaining comfort. The operation costs reductions achieved can be directly attributed to the established coordination mechanism. The results have shown that the software-based coordination between BEMS levels offers the possibility to transform the building energy consumption profile and to reduce the building peak power consumption without large financial investments in the installation of energy storage systems. The hierarchical control presented can be further extended for the provision of demand response services for energy grid entities as well as for the cooperation between buildings within energy communities.

References

[1.] F. Tahersima, J. Stoustrup, H. Rasmussen, and S. A. Meybodi. Economic COP optimization of a heat pump with hierarchical model predictive control. In 2012 51st IEEE Conference on Decision and Control, pages 7583-7588, Dec 2012.

[2.] D. Setlhaolo, S. Sichilalu, and J. Zhang. Residential load management in an energy hub with heat pump water heater. Applied Energy, 208:551-560, 2017.

[3.] F. Oldewurtel, D. Sturzenegger, G. Andersson, M. Morari, and R. S. Smith. Towards a standardized building assessment for demand response. In 2013 52nd IEEE Conference on Decision and Control, pages 7083-7088, 2013.

[4.] K. Klein, S. Herkel, H. M. Henning, and C. Felsmann. Load shifting using the heating and cooling system of an office building: Quantitative potential evaluation for different flexibility and storage options. Applied Energy, 203:917-937, 2017.

[5.] T. T. Gorecki, L. Fabietti, F. A. Qureshi, and C. N. Jones. Experimental demonstration of buildings providing frequency regulation services in the Swiss market. Energy and Buildings, 144:229-240, 2017.

[6.] M. Vašak, A. Banjac, N. Hure, H. Novak, D. Marušić, and V. Lešić. Modular hierarchical model predictive control for coordinated and holistic energy management of buildings, in IEEE Transactions on Energy Conversion (Early Access), 2021.

[7.] V. Lešić, A. Martinčević, and M. Vašak. Modular energy cost optimization for buildings with integrated microgrid. Applied Energy, 197:14-28, 2017.

[8.] F. Borrelli, A. Bemporad, and M. Morari. Geometric algorithm for multiparametric linear programming. Journal of Optimization Theory and Applications, 118(3):515-540, 2003.

[9.] EPEX SPOT. European Power Exchange Electricity Index. Available: http://www.epexspot.com.

Branimir Novoselnik[1], *Mato Baotić*[1]

Electrical Power Distribution System Reconfiguration: Case Study of a Real-life Grid in Croatia

[1] University of Zagreb, Faculty of Electrical Engineering and Computing, Department of Control and Computer Engineering, Laboratory for Renewable Energy Systems, Unska 3, 10000 Zagreb, Croatia

Abstract

This paper describes the application of a nonlinear model predictive control algorithm to the problem of dynamic reconfiguration of an electrical power distribution system with distributed generation and storage. Power distribution systems usually operate in a radial topology despite being physically built as interconnected meshed networks. The meshed structure of the network allows one to modify the network topology by changing the status of the line switches (open/closed). The goal of the control algorithm is to find an optimal radial network topology and optimal power references for controllable generators and energy storage units that will minimize cumulative active power losses while satisfying all system constraints. The validation of the developed algorithm is conducted in a case study of a real-life distribution grid in Croatia. Realistic simulations show that large loss reductions are feasible (more than 13%), i.e., the developed control algorithm can contribute to significant savings for the grid operator.

Keywords: *model predictive control, power distribution system reconfiguration, mixed-integer programming, real-life case study.*

1. Introduction

The ever-increasing demands for electrical energy, limited conventional fuel reserves, climate change, the desire for energy independence and the diversification of energy sources put in focus the distributed production of electrical energy from renewable sources as a key element in achieving sustainable development. Since most of the electricity generated in developed countries is consumed in households, buildings, and industry (see e.g. [9]), the idea is to bring the distributed energy production closer to the end-consumers, i.e., to the power distribution level of the overall electrical power system. Hence, the power distribution system ceases to be a passive part of the electrical power system and starts to be actively involved in the production of electrical energy.

Despite all the advantages of distributed production of electrical energy, the rapidly growing penetration of intermittent renewable energy sources and other distributed sources poses vast challenges for electricity distribution systems ([4]). The challenges mostly relate to the maintenance of grid stability while adhering to the grid codes to ensure reliable and efficient power supply to all consumption entities spatially distributed across the distribution grid. Thus, an active grid management strategy is of key importance in achieving the promised benefits of smart grids – reduction of electricity losses, integration of renewable generation and storage units, reduced use of fossil fuels, and improved grid reliability.

Power distribution systems are built as interconnected meshed networks but they, as a rule, operate in a radial topology. The topology of the network can be modified by changing the open/closed status of line switches which offers additional possibilities for the optimal management of the overall system. Merlin et. al in [6] were the first to emphasize the importance of distribution system reconfiguration (DSR) as an active grid management technique. The DSR problem can generally be modeled as a Mixed-Integer Nonlinear Program (MINLP). Historically, most of the methods for network reconfiguration relied on heuristics ([6]) and artificial intelligence techniques ([2],[5]). Although these algorithms are generally easy to implement and sometimes very fast on practical networks, global solution optimality is not guaranteed and cannot be formally verified. Furthermore, most of the DSR problem formulations do not consider the dynamics of the system.

In contrast to the existing literature, the authors in [7] proposed a closed-loop nonlinear model predictive control (NMPC) algorithm that can take into account system dynamics and its constraints. The NMPC algorithm builds on ideas from [1] and [3]. However, in [7] a simplified, small-scale example is used to illustrate the performance of the NMPC algorithm.

In this paper we validate the developed NMPC algorithm for the dynamic reconfiguration of the distribution grid on a realistic case study of a real-life distribution grid from Koprivnica, Croatia. The NMPC algorithm is implemented in Matlab and tested in real-time using data provided by the grid operator HEP-ODS.

The rest of this paper is organized as follows. The control problem considered herein is formulated in Section 2. In

Section 3 a case study of a real-life power distribution grid in Koprivnica, Croatia, is described. A technical description of the algorithm implementation is given in Section 4. The simulation results are reported in Section 5. Concluding remarks are given in Section 6.

2. Nonlinear MPC formulation

Consider a power network represented by the graph G=($\mathcal{V}$, $\mathcal{E}$), where $v:=\{1,2,...,n\}$ is the set of nodes, and $\mathcal{E}\subseteq\mathcal{V}\times\mathcal{V}$ is the set of flow lines (i,j), where $i,j\in\mathcal{V}$ and $i\neq j$. Each node, except the substation node (i=1), may have loads connected to them. The network has a meshed structure, but it operates radially. It is assumed that all lines are equipped with switches and can participate in the reconfiguration of the network topology.

The control objective is to minimize the total active power losses over a prediction horizon N, i.e., $t\in\{0,1,...N-1\}$. The network losses are equal to the difference between the total system active power generation and the total system active power demand. Consequently, the active power losses of the network at time instant t can be computed as the sum of the total active power injections ($P^I_{i,t}$) at all nodes:

$$P_t^{loss}=\sum_{i\in\mathcal{V}}P^I_{i,t}. \tag{1}$$

The overall nonlinear MPC (NMPC) problem can be formulated as follows:

$$\begin{aligned}\min_x \sum_{t=0}^{N-1} P_t^{loss}(x)\\ s.t.\ g(x)=0,\\ f(x)\le 0,\end{aligned} \tag{2}$$

where x is a vector of all decision variables $V_{i,t}$ (voltage magnitude), $\theta_{i,t}$ (voltage angle), $\delta_{i,t}$ (line switching status), P_t^s (active power injection at substation node), Q_t^s (reactive power injection at substation node), on a prediction horizon of length N. All power injections represent the average power during a discretization interval. Furthermore, all operational and physical constraints, i.e., power balance constraints, voltage constraints, constraints that ensure the radiality of the grid topology, etc., are included in constraints of the optimization problem (2). Since $\delta_{i,t}$ are binary variables, (2) is a mixed-integer non-linear optimization problem but it can be approximated as a mixed-integer linear program (MILP). More details on the control problem formulation can be found in [7].

In closed loop, the NMPC problem (2) is solved at any time instant and only the first control action is applied to the system. At the next time instant, (2) is solved again from the new initial state, according to the receding horizon control strategy (see e.g. [8]).

Even though the available solvers for mixed-integer linear programs are very mature, mixed-integer problems are still generally NP-hard, meaning that attempting to solve them can very easily lead to demanding (and often intractable) computations. Namely, even the state-of-the-art algorithms implemented in commercial solvers like CPLEX have exponential complexity since in the worst case every possible combination of integer variables has to be checked. To alleviate this drawback, we keep the number of binary variables in our problem formulation as low as possible. To achieve this, the number of topology changes on a prediction horizon was limited to only one, i.e., for steps $k=0$ to $k=j-1$ the previous topology is kept and on step $k=j$ a new topology is determined that is to be used until the end of the prediction horizon. Obviously, N such MILP problems can be defined for all $j=0$ to $j=N-1$, where N is the length of the prediction horizon. Moreover, these MILP problems can be solved in parallel and then the solution that generates the minimal cumulative cost on a prediction horizon is chosen.

The limitation of only one topology change on a prediction horizon is also motivated by practical reasons. It is not desirable to use the switching gear too often to prolong its life cycle, so it makes sense to limit the number of switching actions on a prediction horizon.

3. Case study

The electrical grid considered in this paper constitutes a part of the electrical power distribution grid in the city of Koprivnica, Croatia. The grid comprises: 28 nodes, 1 transformer station 110/35 kV, 2 transformer stations 35/10 kV, 3984 consumers, which are modelled as 22 aggregated loads, and 28 transmission lines.

The grid data (node data, line data, transformer data; see [10] for details) as well as access to real-time

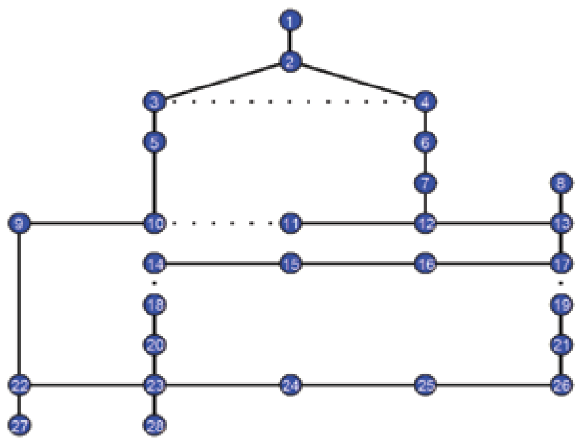

Fig. 1. Graph representation of the distribution grid in Koprivnica.

measurements and historical load profiles at different nodes in the network were provided by the grid operator HEP-ODS.

The graph representation of the Koprivnica distribution grid is shown in Fig. 1. Nodes are represented by blue circles that are numbered from 1 to 28. Lines and transformers that connect nodes are represented as edges of the graph. Full lines represent transmission lines that are switched on, while dotted lines represent transmission lines that are switched off in the current topology. The radial topology depicted in Fig. 1 is the actual topology that was in operation on-site in Koprivnica for four consecutive days. The actual power demand profiles (15-min averages) during those four days in Koprivnica are shown in Fig. 2.

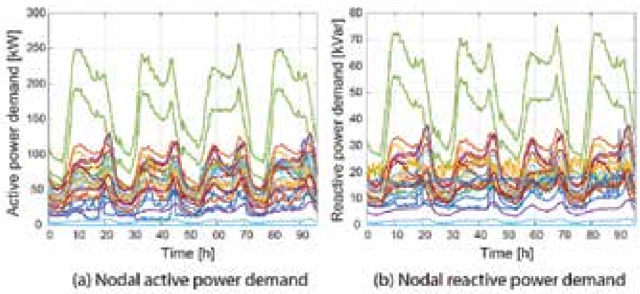

Fig. 2. Nodal power demand profiles in Koprivnica.

4. Simulation results

We ran the following three simulation scenarios:

1.1. In the first simulation run a fixed topology shown in Fig. 1. was kept. This topology was in operation on a real-life power grid in Koprivnica. The results from this simulation are used as a baseline for the following comparisons.

1.2. In the second simulation run the optimal grid topology was computed in each step. Since the grid is in a quasi-static state, there was no need for a prediction horizon. The results of this simulation represent the best that can be achieved by topology reconfiguration in this scenario.

1.3. In the third simulation run, the additional constraint was imposed as follows: only one topology change is allowed on the entire prediction horizon. We used N=6 in our simulation.

All three simulations were run with the entire data set shown in Fig. 2. A time step of 15 minutes was used.

In all three simulations nodal voltage magnitudes were kept safely within the predefined limits of ± 5% around the nominal values (see Fig. 3). For the sake of brevity, we did not include the voltage profiles of other two simulations. The voltages are closer to the upper limit, which makes sense because higher voltages allow for smaller currents in the network and consequently smaller losses.

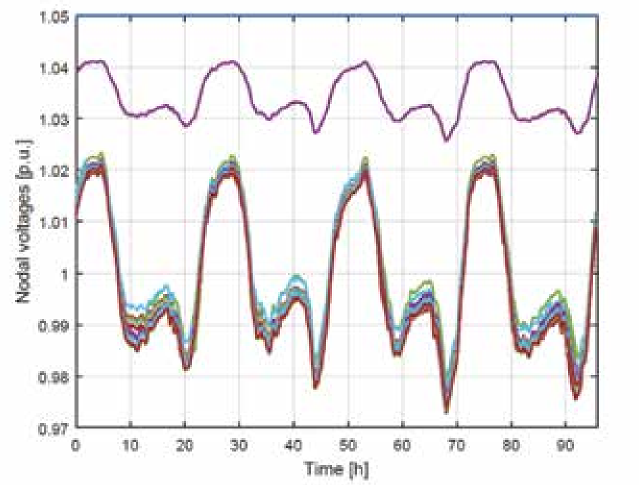

Fig. 3. Nodal voltage magnitudes during simulation 1.3.

The total active power losses during all three simulation runs are shown in Fig. 4. It is evident that in both reconfiguration scenarios a sizable reduction of losses was achieved compared to the baseline scenario where the topology was fixed. Table 1 reports the numeric values of the total active power losses in all three simulations. The losses obtained in simulation runs 1.2 and 1.3 are virtually the same and in both cases the reduction in total losses of around 13.5% compared to the baseline simulation run 1.1 was achieved.

The total number of switching actions per each line in simulations 1.2 and 1.3 are shown in Fig. 5. From this, it is evident that only a handful of lines switched their status on or off over the entire simulation run, while most of the lines never changed their switching status at all. Moreover, some of the lines changed their status rarely, while some of the lines changed their status many times. The total number of switching actions in simulation run 1.2, when the topology was allowed to change in every step, was 158. In simulation 1.3, when the topology could change once in every N steps, this number was 54. Therefore, practically the same performance was achieved with almost three times fewer switching

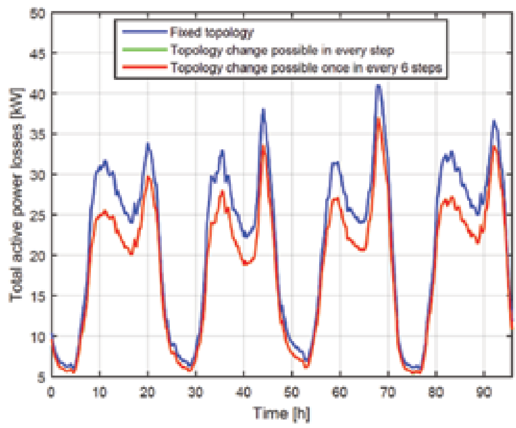

Fig. 4. Total active power losses during all three simulation runs in the scenario 1.

operations, as shown in Table 1. The computation times of the NMPC algorithm in simulations 1.2 and 1.3 are reported in Table 2. Note that the reported computation times for simulation 3 were measured on a single PC solving N MILP problems sequentially in every step of the simulation. In practice, these problems could have been solved in parallel and the computation would have been faster.

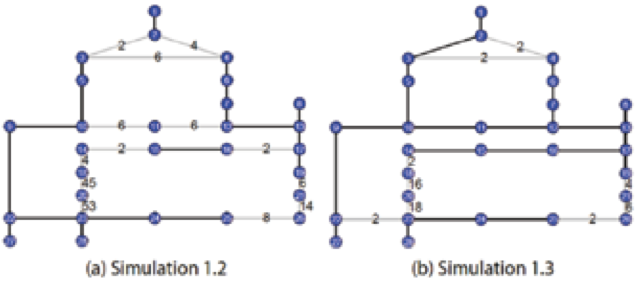

Fig. 5. The total number of switching actions for each line during simulations 1.2 and 1.3.

Table 1. Total active power losses in three simulation runs.

	Total loss [kWh]	Reduction [%]
Simulation 1.1	2068.55	n/a
Simulation 1.2	1788.15	-13.56
Simulation 1.3	1788.48	-13.54

Table 2. Computation times of the NMPC algorithm in simulations 1.2 and 1.3.

	Max [s]	Min [s]	Mean [s]
Simulation 1.2	14.57	2.11	4.81
Simulation 1.3	374.32	100.13	155.02

5. Discussion of results

The presented results of both simulation scenarios 1.2 and 1.3 are very promising and indicate that the applied methods could be implemented in a real-life distribution grid. The most appealing strengths of the method are: (i) process constraints can be systematically taken into account, (ii) certifiably globally optimal solution is obtained in every run of the algorithm, (iii) future power demand and renewable power production profiles can be easily taken into account.

The effectiveness of the reconfiguration depends on the degree of the network automation. In general, the more line switches are available for the dispatcher to change, the higher loss reduction can be achieved, i.e., more different topologies can be considered. In the current grid, the selection of appropriate lines to be updated with the switchgear for remote control of the switch state is based on minimizing a grid fault duration. The results that can be achieved by the reconfiguration algorithm provide an additional benefit to the already existing infrastructure. Consequently, the cost-benefit analysis of the medium voltage level automation system should take this newly added benefit into consideration, which in turn will allow for previously discarded switchgear to be reconsidered for automation. Some of the results presented in this paper provide interesting and valuable information along these lines. In particular, it was assumed in the simulations that all lines are equipped with a switchgear and therefore can change their switch state, although this is not true in the real grid. The results obtained, however, indicate that only some of the lines contributed to the change in the topology during the simulations while other lines never changed their switching state. Obviously, the lines with the highest number of switching actions are natural candidates for possible future upgrades with automatic switchgear in the real-life grid.

A few things should be noted. The algorithm depends on exact knowledge of the future power production and demand profiles. In practice, these profiles can only be predicted, so an accurate predictor is required to enable real-time implementation of the algorithm in a real distribution grid. Furthermore, the algorithm depends on solving a mixed-integer linear program which does not scale well with the size of the problem, i.e., it can easily become very computationally demanding. However, as we have seen in the simulation results, it is not necessary to consider all lines in the grid for topology reconfiguration, because most lines never change their switching status. This means that a smaller number of binary variables is needed to formulate the problem allowing for implementation on even larger power grids.

6. Conclusion

In this paper we have presented the application of an NMPC algorithm for dynamic reconfiguration of power distribution systems in a case study of a real-life power distribution grid in Croatia. The performance of the dynamic reconfiguration algorithm was validated in realistic simulation scenarios using real-life data provided by the grid operator. The results are very promising and show that large loss reductions are feasible (more than 13%). The developed NMPC algorithm has the potential to be applied to a real-life grid and can contribute to significant savings.

References

[1.] Ben-Tal, A. and Nemirovski, A. (2001). On polyhedral approximations of the second-order cone. Math. Oper. Res., 26(2), 193-205.

[2] Carreno, E.M., Romero, R., and Padilha-Feltrin, A. (2008). An effcient codification to solve distribution

network reconfiguration for loss reduction problem. IEEE Transactions on Power Systems, 23(4), 1542-1551.

[3] Jabr, R.A. (2014). Minimum loss operation of distribution networks with photovoltaic generation. IET Renewable Power Generation, 8(1), 33-44.

[4] Keane, A., Ochoa, L.F., Borges, C.L.T., Ault, G.W., Alarcon-Rodriguez, A.D., Currie, R.A.F., Pilo, F., Dent, C., and Harrison, G.P. (2013). State-of-the-art techniques and challenges ahead for distributed generation planning and optimization. IEEE Transactions on Power Systems, 28(2), 1493-1502.

[5] Khan, I. and Ravichandran, S. (2005). Distribution network reconfiguration for loss reduction using ant colony system algorithm. In INDICON, 2005 Annual IEEE, 619-622.

[6] Merlin, A. and Back, H. (1975). Search for a Minimal-Loss Operating Spanning Tree Configuration in an Urban Power Distribution System. In Proc. Power Systems Computation Conference, 1-18.

[7] Novoselnik, B. and Baotic, M. (2015). Dynamic reconfiguration of electrical power distribution systems with distributed generation and storage. IFAC-PapersOnLine, 48(23), 136-141. 5th IFAC Conference on Nonlinear Model Predictive Control (NMPC).

[8] Rawlings, J.B. and Mayne, D.Q. (2009). Model Predictive Control: Theory and Design. Nob Hill Publishing, LLC.

[9] REN21 (2016). Renewables 2016 Global Status Report. Renewable Energy Policy Network for the 21st Century (REN21

[10] Novoselnik, B, Bolfek, M., Bošković, M. and Baotic. M. (2017). Electrical Power Distribution System Reconfiguration: Case Study of a Real-life Grid in Croatia. IFAC-PapersOnLine 50(1), 61-66. 20th IFAC World Congress.

Branimir Brkić[1], Marko Kovačević[1], and Mario Vašak[1]

Worst-Case Optimal Scheduling and Real-Time Control of a Microgrid Offering Active Power Reserve

[1] University of Zagreb, Faculty of Electrical Engineering and Computing, Department of Control and Computer Engineering, Laboratory for Renewable Energy Systems, Unska 3, 10000 Zagreb, Croatia

Abstract

This work is focused on optimization problems within the predictive control framework for determining and engaging the flexibility of a microgrid in grid-microgrid energy exchange. The microgrid has a controllable battery storage and other components represented with a residual power flow. All major economic constituents of the grid-connected microgrid operation are considered: day-ahead, intra-day, peak power and battery degradation costs, as well as rewards and penalties for providing flexibility. The problems are posed as linear worst-case minimization programs in which all flexibility activation scenarios are taken into account. An analysis is conducted for various combinations of flexibility reservation and activation prices that can be bid to a grid entity. The technical and economic feasibility of the flexibility provision is confirmed by the use of an online model predictive controller that optimally meets the requirements of grid flexibility according to the declared reserve in the environment of online occurring disturbances and events.

Keywords: *smart grids, microgrids, linear programming, model predictive control, demand response*

1. Introduction

Frequency regulation as one of the means to ensure optimal functioning of the electrical grid can be divided into three categories based on the response time of the regulation units: primary, secondary and tertiary. Tertiary regulation can be further divided into tertiary regulation for system balancing and tertiary regulation for system safety. This paper focuses on the tertiary regulation of frequency for system balancing achieved through the activation of active power reserves by a transmission system operator (TSO). The TSO accepts or declines the declared power reserve under the offered pricing conditions. In case of acceptance, the entity must change its previously planned and declared electrical load upon the TSO request within a time frame that differs from contract to contract [1]. Usual time frames discussed in this area of research include requests coming as immediate as 15-minute prior to activation according to arrangements for a specific time slot made the day before. In this work we focus on the power reserve activation that can be called by the TSO up to 15 minutes before the activation time according to the declaration made beforehand. This behavior is also termed as explicit demand response – a framework for a TSO or a distribution system operator (DSO) to offer contract deals to electrical energy consumers with the aim of costs reduction on both sides based on flexibility of the end-consumers' consumption [2].

Besides explicit demand response, the electrical energy provider can implicitly influence consumers to reduce peak power during times that are characterized by high electrical energy usage. This is achieved by increasing prices of electrical energy in peak times and decreasing prices when it is strategically appropriate to encourage consumption. Additionally, every electrical energy consumer contractually agrees with the electrical energy provider on a specific maximum power. The consumption above the declared maximum power is penalized by higher electrical energy prices [3].

To allow consumers or prosumers participation in flexibility provision, novel control systems enabling efficient and profitable demand response services have been developed. In [4] frequency regulation system for DR using electric vehicles charging and historical data to determine expectations of stochastic variables is developed. Cost-benefit analyses, using mixed integer linear programming, for several microgrid configurations are given in [5]. Besides a battery storage system, a building thermal mass can also be used as a thermal energy storage that contributes to the building's flexibility in electrical energy consumption planning. The downside of the approach are larger thermal losses compared to the optimal control focused solely on energy-efficiency [6]. The coordinated operation between the building microgrid and the central heating, ventilation and air conditioning system (HVAC) for mutual flexibility provision is explored in our previous work [7].

This paper is a shortened version of the work [8]. Its main contributions are summarized as:

- optimization-based determination of optimal frequency regulation reserve power offer according to commercial rules for flexibility provision by the Croatian TSO,
- real-time Model Predictive Controller (MPC) that assures feasibility of flexibility provision for every possible moment of activation,
- worst-case optimization without stochastic data needed.

The work is organized as follows: Section 2 introduces a considered building microgrid and explains the DR scheme together with its corresponding optimization problem formulation. The simulation results based on a real case-study are elaborated in Section 3 and the conclusion is given in the final section.

2. Formulation of the optimization problem

A. Microgrid description

The considered microgrid consists of a battery storage and a non-controllable consumption combined with a photovoltaic source. Since the microgrid is connected to a distribution grid, its energy exchange with the grid is described with:

$$E_{\mathrm{g}}(k) = u_{\mathrm{ch}}(k) - u_{\mathrm{dch}}(k) + E_{\mathrm{nc}}(k), \quad (1)$$

where positive values of $E_{\mathrm{g}}(k)$ relate to the energy taken from the grid and negative values to the energy provided to the grid, u_{ch} and u_{dch} are controllable battery charging and discharging energies, respectively. Notation E_{nc} stands for the non-controllable energy consumption of the building. All energy variables in discrete-time actually correspond to the energies in time intervals between kT and $(k+1)T$ where T is the discretization time of 15 min. System dynamics is described with only one system state which is the battery state of energy:

$$SoE(k+1) = SoE(k) + \eta u_{\mathrm{ch}}(k) - u_{\mathrm{dch}}(k)/\eta, \quad (2)$$

where η is the efficiency of the battery system (power converter + battery). As in [10], it is possible for the battery to be both charged and discharged within one discretization interval, but respecting the following constraints:

$$\begin{cases} u_{\mathrm{ch}}(k) + u_{\mathrm{dch}}(k) \leq P_{\mathrm{max}}T \\ 0 \leq u_{\mathrm{ch}}(k) \leq P_{\mathrm{max}}T \\ 0 \leq u_{\mathrm{dch}}(k) \leq P_{\mathrm{max}}T \end{cases} \quad (3)$$

where P_{max} denotes the maximum power of the battery power converter (9.6 kW in the considered microgrid).

B. Cost variables

In this subsection components of the microgrid cost function for energy exchange with the grid including DR functionality are introduced. These components include day-ahead energy cost, intra-day energy cost, peak power penalization, frequency regulation reserve power revenue, regulation energy revenue and battery degradation cost.

Consumed electrical energy cost J_{da} is calculated in the following way:

$$J_{\mathrm{da}}(E_{\mathrm{g}}) = \sum_k c_{\mathrm{da}}(k)\, E_{\mathrm{g}}(k) \quad (4)$$

where c_{da} is a vector of day-ahead prices for every 15-min discretization interval, obtained from the supplier or the electricity market.

On the intra-day market, the deviation of the exhibited energy exchange profile E_{g} from the day-ahead predicted/declared reference energy profile $E_{\mathrm{g,ref}}$ is penalized with the cost function:

$$J_{\mathrm{id}}(E_{\mathrm{g}}, E_{\mathrm{g,ref}}) = \sum_k 1.2 c_{\mathrm{da}}(k) \left| E_{\mathrm{g}}(k) - E_{\mathrm{g,ref}}(k) \right| \quad (5)$$

Depending on the optimization problem, $E_{\mathrm{g,ref}}$ is either a profile to be declared to the grid that is an optimization variable or an already declared profile which is then a constant parameter.

The microgrid contracts peak power $P_{pp,c}$ to the grid on monthly basis. The peak power cost considered in this paper is derived based on the peak power billing in Croatia [9], [10] and is defined with

$$J_{pp}(E_g) = c_{pp}\varepsilon_{pp}, \quad \text{s.t.} \begin{cases} \varepsilon_{pp} \geq \varepsilon_{pp,past}, \\ \varepsilon_{pp} \geq 0.85P_{pp,c}, \\ \varepsilon_{pp} \geq E_g(k)/T, \\ \varepsilon_{pp} \geq 3E_g(k)/T - 2.1P_{pp,c}, \end{cases} \quad (6)$$

where $\mathcal{E}_{pp}$ is an auxiliary variable and c_{pp} is the price of peak power obtained from the grid operator.

The microgrid contracts unique reserve power P_{res} for every day in the next week and it is rewarded with

$$J_{res}(P_{res}) = \sum_d c_{res}\mathrm{sgn}(P_{res}(d))\,P_{res}(d), \quad \forall d \in \mathcal{W} \quad (7)$$

where $c_{res} \leq 0$ is the price of reserve active power and $\mathcal{W}$ denotes the set of indices of days in a week. Since reserve power market is performed as an auction, choosing c_{res} is out of the scope of this paper and the reader can find more about this problem in e.g. [11].

If the grid activates a part of or the whole agreed flexibility reserve, which can last up to two hours, the microgrid is rewarded for the exhibited difference in electrical energy consumption compared to the declared consumption:

$$J_{act}(E_g, E_{g,ref}, P_{act}, i) = \sum_k c_{act}\varepsilon_{act}(k), i \leq k < i+8 \quad (8)$$

$$\text{s.t.} \begin{cases} \varepsilon_{act}(k) \leq \mathrm{sgn}(P_{act})(E_g(k) - E_{g,ref}(k)) \\ \varepsilon_{act}(k) \leq \mathrm{sgn}(P_{act})P_{act}\mathrm{T} \\ \varepsilon_{act}(k) \geq \mathrm{sgn}(P_{act})(1-\alpha)P_{act}\mathrm{T} \end{cases} \quad (9)$$

where P_{act} is a regulation power request of the grid that must be of the same sign and in absolute value lower than the absolute value of P_{res}, $\mathcal{E}_{act}$ is an auxiliary variable, $\mathbf{c_{act}}$ is the price of regulation energy, α=0.25 is a tolerance factor.

Battery capacity is degraded by every charging and discharging action which is penalized with:

$$J_{bd}(u_{ch}, u_{dch}) = \sum_k c_{bd}(u_{ch}(k) + u_{dch}(k)) \quad (10)$$

where $\mathbf{c_{bd}}$ is the battery degradation cost [12].

C. Offline analysis optimization problem

The considered optimization problem consists of one scenario S_i for the activation at every possible discretization interval i in a day ($i \in \mathcal{H}, \mathcal{H} = \{0,1,...,95\}$) and of a scenario S_n without activation. Further on, indices i and n are used with different variables to denote a scenario to which a particular variable belongs. The information about the activation at the moment i is available just at the interval i–1 which means that all states of the scenario S_i must be equal to the ones of the scenario S_n when the activation occurs. Such an optimization problem can be qualified as the worst-case multi-stage recourse problem according to [13].

Constraints that connect scenarios S_n and S_i assure that all decision variables are calculated using only information available at the corresponding moment:

$$SoE_i(k) = SoE_n(k) \forall k \in \{i + 96d | d \in \mathcal{W}, i \in \mathcal{H}\} \quad (11)$$

Scenario S_i contains seven activations at the i^{th} adiscretization interval each day (every 24 h), which is athe most frequently possible and the scenario S_n does anot contain any activation. Altogether there are 97 ascenarios. Total costs J_n of scenario without activation aand J_i of scenarios with activation at interval i are adefined as:

$$J_n = J_{da}(E_{g,n}) + J_{pp}(E_{g,n}) + J_{bd}(u_{ch,n}, u_{dch,n}) \quad (12)$$

$$J_i = J_{da}(E_{g,i}) + J_{pp}(E_{g,i}) + J_{bd}(u_{ch,i}, u_{dch,i}) + J_{id}(E_{g,i}, E_{g,n}) + \sum_d J_{act}(E_{g,i}, E_{g,n}, P_{res,d}, i + 96d) \quad (13)$$

It can be seen from (13) that every scenario assumes the grid will activate the whole contracted reserve power P_{res} . The optimization variables of the offline problem, besides the auxiliary variables from (6), (8) and (9), are u_{ch}, u_{dch}, $P_{pp,c}$ and $SoE(0)$ of all scenarios and the vector of contracted daily regulation power reserve P_{res} while the cost being minimized is:

$$J^*_{offline} = \min_{u_{ch}, u_{dch}, SoE(0), P_{pp,c}, P_{res}} J_{res} + J_{worst} \quad (14)$$

$$\text{s.t.} \begin{cases} J_{worst} \geq J_n, \\ J_{worst} \geq J_i, \forall i \\ (1) - (13) \end{cases} \quad (15)$$

D. Online MPC optimization problem

Online MPC operates in receding horizon fashion with a sampling time T = 15 min and applies only the optimal control variables for the first time-instant k, $u_{ch,n}(0)$ and $u_{dch,n}(0)$, to the battery storage system.

Contrary to the offline formulation, J_{act} is defined as follows for the online formulation:

$$J_{act}(E_g, E_{g,ref}, P_{act}, i) = \sum_k c_{act}\varepsilon_{act}(k) + \sum_k c_s\,\varepsilon_{s1}(k), \quad i \leq k < i+8, \quad (16)$$

$$\text{s.t.}\begin{cases}\varepsilon_{\text{act}}(k) \le \text{sgn}(P_{\text{act}})\left(E_{\text{g}}(k) - \gamma(i,k)E_{\text{g,ref}}(k)\right), \\ \varepsilon_{\text{act}}(k) \le \text{sgn}(P_{\text{act}})P_{\text{act}}T, \\ \varepsilon_{\text{act}}(k) + \varepsilon_{\text{s1}}(k) \ge \text{sgn}(P_{\text{act}})(1-\alpha)P_{\text{act}}T, \\ \gamma(i,k) = \begin{cases}\dfrac{\sum_{j=-4}^{1} E_{\text{g}}(i+j)}{\sum_{j=-4}^{1} E_{\text{g,ref}}(i+j)}, k \le k_{\text{mid}} \\ 1, k > k_{\text{mid}}\end{cases},\end{cases} \tag{17}$$

The introduced auxiliary variable $\mathcal{E}_{s1}$ and its contribution to J_{act} are an implementation of soft constraints to enable feasibility of the optimization problem even if the microgrid cannot fulfill activated regulation power due to an unfavorable noncontrollable consumption. Soft constraint penalty is taken as $c_s=10^5$.

Both the declared consumption profile E_g^* and the profile that is going to be declared $E_{g,n}^+$ are used as a reference profile in (16), depending on the discretization interval k. The prediction horizon in on-line MPC always corresponds to the length of known day-ahead prices. When the prices for the following day are announced, the online MPC abruptly increases the prediction horizon for another 24 hours and declares the solution $E_{g,n}^+$ for the following day to the grid. Notation k_{mid} denotes the last discretization interval with the known declared consumption profile. To avoid non-linearity and the need for a sequential linear program it is assumed that after k_{mid}, γ is equal to 1 as the worst case, and thus an auxiliary cost J_{aux} and constraints are added to scenario S_n:

$$J_{\text{aux}}(E_{\text{g,n}}, E_{\text{g,ref}}) = \sum_{k} c_{\text{s}}\varepsilon_{\text{s2}}(k), \tag{18}$$

$$\text{s.t.}\begin{cases}\text{sgn}(P_{\text{res}})\left(E_{\text{g,n}}(k) + \varepsilon_{\text{s2}}(k)\right) \le \text{sgn}(P_{\text{res}})E_{\text{g,ref}}(k) \\ \varepsilon_{\text{s2}}(k) \ge 0, \\ \forall k \in \{k_{\text{mid}} - 10, \dots, k_{\text{mid}}\}\end{cases} \tag{19}$$

All cost functions are the same as in the offline problem except J_{act} which is then added to (12) and (13), and also J_{aux} and J_{id} ($E_{g,n}^-$, E_g^*) are added to (12).

The final problem to be solved is

$$J_{\text{online}}^* = \min_{u} J_{\text{worst}} \tag{20}$$

$$\text{s.t.}\begin{cases}J_{\text{worst}} \ge J_{\text{n}}, \\ J_{\text{worst}} \ge J_i, \forall i \\ (1)-(6), (10)-(13), (16)-(19)\end{cases} \tag{21}$$

where u denotes the charging and discharging signals of all scenarios.

3. Simulation

A. Offline analysis

In the following section, offline analysis is conducted to ascertain how the agreed activation and reservation prices between the TSO and the microgrid affect operational costs of the microgrid, based on historical data E_{nc} and c_{da}.

In Table I, several combinations of activation prices and reservation prices are shown for the maximum activation duration of one and two hours, respectively. To make sure that the reserved powers are at their maximum and uniform across all seven days, it is recommended to raise the reservation price instead of the activation price to further increase the optimal reserved powers. Of the other results listed in the table, $\bar{J}$ denotes the mean cost of all scenarios, and J_{worst} denotes the highest cost value among all the scenarios that generally corresponds to the scenario S_n since it does not contain the activation reward J_{act}.

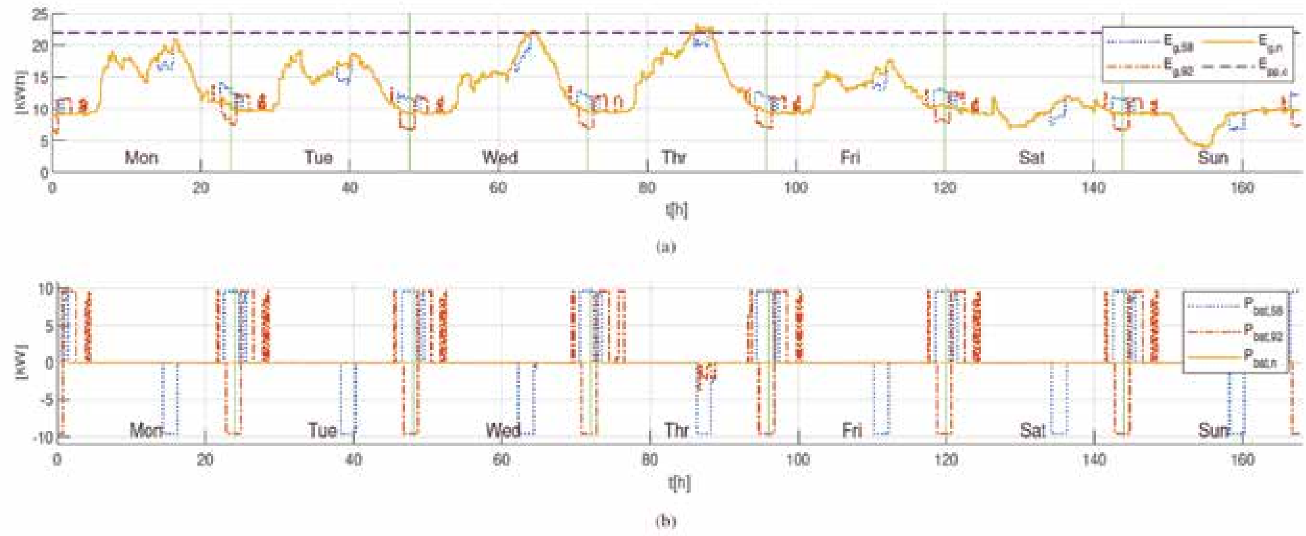

Fig. 1: Results of offline analysis. (a) energy exchange with the grid and (b) battery charging power ($P_{bat} = \frac{u_{ch}-u_{dch}}{T}$).

TABLE I: Offline analysis results.

Prices	P_{res}[kW]	$\overline{J}$[€]	J_{worst}[€]
$c_{\mathrm{act}} = -0.4$ €/kWh $c_{\mathrm{res}} = -0.1$ €/kW, 1h	[-12.8, -12.8, -9.85, -5.23, -12.8, -12.8, -12.8]	617.34	621.83
$c_{\mathrm{act}} = -0.4$ €/kWh $c_{\mathrm{res}} = -0.7$ €/kW, 1h	[-12.8, -12.8, -12.8, -12.8, -12.8, -12.8, -12.8]	563.88	570.63
$c_{\mathrm{act}} = -0.4$ €/kWh $c_{\mathrm{res}} = -0.1$ €/kW, 2h	[-12.8, -12.8, -9.85, -5.23, -12.8, -12.8, -12.8]	613.17	621.47
$c_{\mathrm{act}} = -0.4$ €/kWh $c_{\mathrm{res}} = -0.7$ €/kW, 2h	[-12.8, -12.8, -12.8, -12.8, -12.8, -12.8, -12.8]	559.64	570.25
without DR			625.64

Fig. 1a. shows energy exchange with the grid for a period of seven days with a time resolution of 15-minutes. It can be noticed that the energy exchange profile $E_{\mathrm{g,n}}$ does not include any charges or discharges of the battery because this strategy enables the microgrid to fulfill all the activations in scenarios S_i. In Fig. 1b, it can also be noticed that the batteries in the scenarios S_i tend to charge when the electricity prices are low (usually around midnight) and discharge to their full extent (2 hours and 75% of the reserved power in the particular simulation) when they are activated. The activation that starts around midnight of the last day is circled back to the first day in the optimization problem to satisfy the repeatability condition of the battery's *SoE*.

Contracted peak energy $E_{\mathrm{pp,c}} = P_{\mathrm{pp,c}}T$ can also be found in the graph (purple dashed). It is chosen so that the peak power of scenario S_{n} is on the edge of the interval where there are no penalties, i.e. it does not cross 105% of $P_{\mathrm{pp,c}}T$. The energy exchange profile $E_{\mathrm{g,92}}$ of the scenario S_{92} (flexibility activation at 22:45 every day) uses the battery to reduce the maximum total peak power while profile $E_{\mathrm{g,58}}$ exhibits flexibility activation at the same time.

B. Online MPC

One pair of prices $c_{\mathrm{res}}=-0.7$ EUR/kW and $c_{\mathrm{act}}=-0.4$ EUR/kWh and the calculated optimal $P_{\mathrm{res}}=-12.8$ kW are taken for a case study simulation of the online MPC.

The simulation results are shown in Figs. 2a and 2b. In the online simulation optimization is run in every discretization interval and all signals are marked with a suffix denoting the interval when they are obtained. The number in the index denotes a scenario relative to the interval while $E^{\square}_{\mathrm{g,cl}}$ denotes the exhibited energy exchange profile obtained with the closed-loop MPC.

It can be seen how the microgrid changes its plan during the time. At the beginning of the simulation the microgrid decides to charge the battery around midnight in the case of scenario $i = 52$ (dashed dark blue line $E^{0}_{\mathrm{g,52}}$ and $P^{0}_{\mathrm{bat,52}}$). Midnight battery charging corresponds to the low energy prices period and it is within the recuperation period, assuring the microgrid will be ready for every possible next activation.

After the activation occurred at $k = 52$ (13:00) the microgrid does not have to be ready for an activation until $k = 52 + 96$ and reference profile $E^{*}_{\mathrm{g,d+1}}$ is not declared until 17:00. The microgrid exploits that situation to postpone charging to expiration of the recuperation period which can be seen by observing $E^{*}_{\mathrm{g,d+1}}$ (yellow dashed line). Thus the microgrid reduced the battery degradation cost for the first several scenarios after the recuperation period, which is considerably more than a difference in electrical energy prices. Not only frequency regulation is fully fulfilled without discharging the battery but also one charging cycle is avoided. Furthermore, even if the next activation is after the rescheduled charging (i.e. after 40 h), the microgrid still achieved savings by avoiding intra-day costs that would occur in the case of midnight charging.

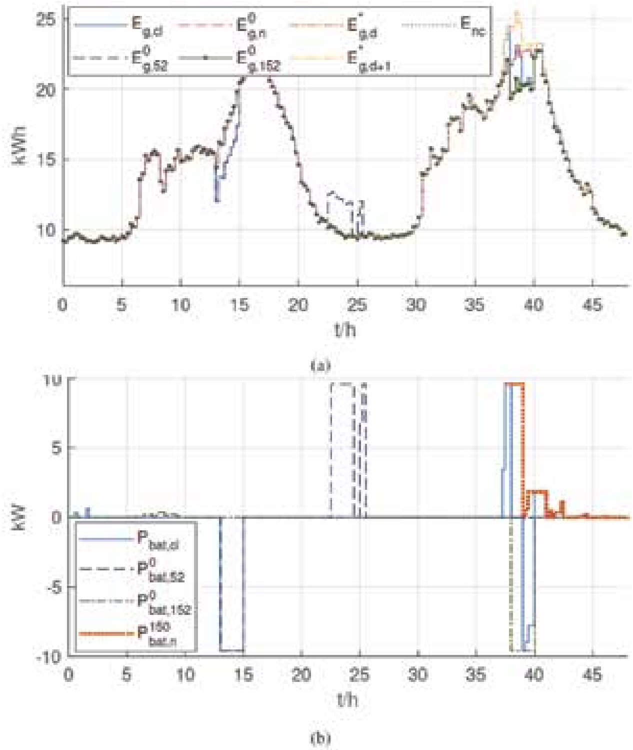

Fig. 2: Simulation results for real-time MPC. (a) energy exchange with the grid and (b) battery charging power ($P_{\mathrm{bat}} = \frac{u_{\mathrm{ch}} - u_{\mathrm{dch}}}{T}$).

4. Conclusion

This paper deals with the building microgrid's ability to participate in tertiary frequency regulation through demand response and obtaining benefits by the predictive control of battery charging and discharging. At the same time additional benefits are assured through peak power reduction and participation in the day-ahead energy market. Furthermore, the building contributes to better grid operation and power system regulation.

Acknowledgment

This work was supported by European Union Regional Development Fund via Operational Programme Competitiveness and Cohesion for Croatia through the Project PC-ATE Buildings – Development of a System for Predictive Control and Autonomous Trading of Energy in Buildings under Contract KK.01.2.1.01.0069.

References

[1.] Croatian Transmission System Operator. (2020) Demand side response. [Online]. Available: https://www.hops.hr/en/demand-side-response

[2] P. Zancanella, P. Bertoldi, and B. Kiss, "Demand response status in EU member states," Publications Office of the European Union, 2016.

[3] B. Brkić and M. Vašak, "Analysis of a diesel-generator-assisted peak power reduction in a production plant," in 2020 IEEE 11th International Symposium on Power Electronics for Distributed Generation Systems (PEDG), 2020, pp. 242–246.

[4] E. Sortomme and M. A. El-Sharkawi, "Optimal scheduling of vehicle-to-grid energy and ancillary services," IEEE Transactions on Smart Grid, vol. 3, no. 1, pp. 351–359, 2012.

[5] F. Marangoni, L. Magatao, and L. de Arruda, "Demand response optimization model to energy and power expenses analysis and contract revision," Energies, vol. 13, no. 11, p. 2803, 2020.

[6] L. Kreuder and C. Spataru, "Assessing demand response with heat pumps for efficient grid operation in smart grids," Sustainable Cities and Society, vol. 19,pp.136-143, 2015. [Online]. Available: http://www.sciencedirect.com/science/article/pii/S2210670715300159

[7] M. Kovačević, D. Marušić, and M. Vašak, "Price-optimal electrical and thermal energy flow control within microgrid – smart grid interaction", in 2020 IEEE 11th International Symposium on Power Electronics for Distributed Generation Systems (PEDG), 2020, pp. 247–252.

[8] M. Kovačević, B. Brkić, and M. Vašak, "Worst-case optimal scheduling and real-time control of a microgrid offering active power reserve," 2021 23rd International Conference on Process Control (PC), 2021, pp. 66-71, doi: 10.1109/PC52310.2021.9447502.

[9] Croatian Energy Regulatory Agency. (2020) Distribution system tariff. [Online]. Available: https://zakon.poslovna.hr/public/tarifni-sustav-za-distribuciju-elektricne-energije%2C-bez-visine-tarifnih-stavki/409408/zakoni.aspx

[10] HEP-Operator distribucijskog sustava d.o.o. (2020) Distribution system prices. [Online]. Available: https://www.hep.hr/ods/kupci/poduzetnistvo/tarifne-stavke-cijene-161/161#

[11] M. Shafie-khah, M. Moghaddam, M. Sheikh-El-Eslami, and J. Catalao, "Optimised performance of a plug-in electric vehicle aggregator in energy and reserve markets," Energy Conversion and Management, vol. 97, pp. 393 – 408, 2015.

[12] F. Rukavina and M. Vašak, "Optimal parameterization of a PV and a battery system add-on for a consumer," in 2020 IEEE 11th International Symposium on Power Electronics for Distributed Generation Systems (PEDG), 2020, pp. 621–626.

[13] J. Murphy, "Benders, nested benders and stochastic programming: An intuitive introduction," 2013. [Online]. Available:https://arxiv.org/abs/1312.3158v

Filip Rukavina[1], *Mario Vašak*[1]

Parameterization of a Photovoltaic and a Battery System Add-On for a Consumer Based on a Sequential Linear Program

[1] University of Zagreb, Faculty of Electrical Engineering and Computing, Department of Control and Computer Engineering, Laboratory for Renewable Energy Systems, Unska 3, 10000 Zagreb, Croatia

Abstract

This paper describes a procedure for optimal sizing of the investment in a renewable electricity source and electricity storage for a particular consumer with a known electricity consumption profile, under the given conditions of allowed return on investment period and with the optimal operation of the battery storage system included. The optimal size of the PV system in terms of its power production under standard test conditions is provided, as well as the optimal size of the battery storage system in terms of its power converter power rating and the storage capacity. The procedure is based on a sequential linear programming method which enables the computations tractability on regularly sized computers.

Keywords: *optimal sizing, sequential linear programming, photovoltaic system, battery energy storage system*

1. Introduction

Energy storage is nowadays recognized as a key element in a modern energy supply chain. This is mainly because it can enhance grid stability, increase penetration of renewable energy resources, improve the efficiency of energy systems, conserve fossil energy resources and reduce environmental impact of energy generation

[1]. Furthermore, energy storages in combination with renewable energy sources can significantly reduce a consumer's electricity bill [2].

Because of the mature technologies, ease of use and installation, and relatively low prices, photovoltaic (PV) and battery energy storage systems (BESSs) are a good choice for a renewable energy source and energy storage solution. A procedure is proposed to support the design process of those systems for a new consumer. Unlike in [3] and [4] where authors used evolutionary algorithms to find (near) optimal parameters, this procedure uses a sequential/successive linear programming (SLP) method to determine parameters of the PV system and the BESS close to true optimal values. Those parameters are the peak power of the PV system, energy capacity of the BESS and maximum power of the BESS power converter. Peak power of the PV system is provided in terms of its power production under standard test conditions (STC): 1000 W/m^2 input irradiance and 25°C PV modules temperature.

The prices for feed-in energy are considerably low compared to the prices for energy coming from the utility grid. This difference in prices does not bring any cost benefit to the consumer when selling the excess of energy to the utility company. Therefore, the procedure focuses on net-zero rather than on net-positive approach. The goal is to keep the consumer as independent as possible of the utility, i.e. to have as little as possible energy exchange with the utility. That way the electricity bill for the consumer is minimized. The greater the difference in price between buying and selling the energy, the lower is the payback period when buying a BESS along with a PV system.

The similar procedure is described in [5], where the optimization consists of a single linear programming (LP) problem. However, such an LP problem is too large to be solved on a regular computer which is a targeted hardware for this procedure, as it is a part of an energy management tool freely available at [6]. This procedure, in contrast to the one described in [5], uses a SLP method where a series of smaller LP problems are solved which results in a somewhat slower execution but in significantly lower hardware requirements.

The rest of this paper is organized as follows. The procedure considered herein is formulated in Section 2. In Section 3 the results for a real-life consumer are presented. Concluding remarks are given in Section 4.

2. Procedure formulation

The mentioned optimal parameters are computed based on the measured electrical energy consumption at the consumer's grid connection point, and a PV energy production. As the PV system is yet to be installed, global solar irradiance measurements and sun angles (elevation and azimuth) during the year are used. Together with orientation and inclination angles of the planned PV solar arrays, a possible PV production profile, P_{PV}, is generated by scaling a reference profile $P_{\mathrm{PV},ref}$.

Instead of solving one large LP problem,

$$\begin{aligned} &\min_x f^T x \\ s.t.\ &A_{\mathrm{ineq}} x \le b_{\mathrm{ineq}}, \\ &A_{\mathrm{eq}} x = b_{\mathrm{eq}}, \\ &x_{\min} \le x \le x_{\max}, \end{aligned} \tag{1}$$

the result is obtained by solving a series of smaller LP problems, i.e. by utilizing a SLP method, where solving one LP is called iteration. Iterations are separated into:

- Initial iteration (1 iteration),
- Efficiency and degradation iteration (1 iteration),
- Feed-in price iterations (≥1 iterations),
- Converging iterations (≥1 iterations).

The calculation process can be stopped in any iteration if the PV and BESS turn out to be economically non-viable.

Initial iteration

In the initial iteration, the state of energy of the battery, SoE, is influenced by BESS charging (or discharging) power, P_{bat}, without efficiency included, i.e. it is considered that there are no energy losses:

$$SoE(k+1) = SoE(k) + P_{\mathrm{bat}}(k) T_{\mathrm{s}} \tag{2}$$

where T_{s} is the sampling time and P_{bat} is positive while charging, and negative while discharging. The power exchange with the utility grid is calculated as

$$\begin{aligned} P_{\mathrm{grid}}(k) = P_{\mathrm{dem}}(k) + P_{\mathrm{bat}}(k) \\ - \alpha_{\mathrm{PV}} P_{\mathrm{PV},ref}(k), \end{aligned} \tag{3}$$

where α_{PV} is a scaling coefficient used to calculate the optimal peak power of the new PV system with respect to the one obtained from the known solar irradiance profile.

The cost function, $f(x)$, which is minimized by solving each of the LP problems, equals the price of the energy exchange with the utility grid $J_{\mathrm{yes,inv}}$:

$$\begin{aligned} J_{\mathrm{yes,inv}} = c_{\mathrm{grid}} \sum_{k=0}^{N-1} P_{\mathrm{grid}}(k) T_{\mathrm{s}} \\ + c_{\mathrm{peak}} \sum_{l=1}^{12} P_{\mathrm{peak}}(l) \end{aligned} \tag{4}$$

where c_{grid} is the price of electricity from the utility grid, N is the length of the horizon, c_{peak} is the price of the monthly peak power, and P_{peak} is the monthly peak power.

Before defining the optimization vector and the constraints, two more variables need to be defined: the cost of the investment denoted by J_{inv}, and the cost of yearly maintenance denoted by J_{ym}.

$$\begin{aligned} J_{\mathrm{inv}} = c_{\mathrm{bat}} SoE_{\max} + c_{\mathrm{pc}} P_{\mathrm{pc,max}} \\ + c_{\mathrm{PV}} P_{\mathrm{PV,peak},ref} \alpha_{\mathrm{PV}}, \end{aligned} \tag{5}$$

$$J_{\text{ym}} = \frac{c_{\text{bat}}}{n_{\text{bat}}} SoE_{\max} + \frac{c_{\text{pc}}}{n_{\text{pc}}} P_{\text{pc,max}} + \frac{c_{\text{PV}}}{n_{\text{PV}}} P_{\text{PV,peak,ref}} \alpha_{\text{PV}}, \tag{6}$$

where c_{bat} is the price of the battery pack per unit of energy capacity, $SoE_{\max}$ is the energy capacity of the battery, n_{bat} is the lifetime of the battery pack in years, c_{pc} is the price of the power converter per unit of power, $P_{\text{pc,max}}$ is the nominal power of the power converter, n_{pc} is the lifetime of the power converter in years, c_{PV} is the price of the PV system per unit of the installed power, and n_{PV} is the lifetime of the PV system in years.

The length of the prediction horizon is N, while the optimization vector x consists of:

- charging/discharging powers of the BESS, $P_{\text{bat}}(k)$, $k \in [0 \dots N-1]$;
- monthly peak power of power exchange with the grid, $P_{\text{peak}}(l)$, $l \in [1 \dots 12]$;
- starting state of energy of the battery, $SoE(0)$;
- energy capacity of the battery pack, $SoE_{\max}$;
- nominal power of the power converter, $P_{\text{pc,max}}$;
- scaling coefficient of the PV system, α_{PV}.

To fully construct the LP problem (1) and to fully describe the overall system mathematically, equality and inequality constraints must be posed. The only equality constraint makes sure that the calculated sequence is repeatable, i.e. the last instance of the BESS state of energy must be equal to the starting one:

$$SoE(0) = SoE(N). \tag{7}$$

Inequality constraints, inter alia, make sure that:

- the battery is never under- nor over-charged,

$$(1 - DoD) SoE_{\max} \le SoE(k) \le SoE_{\max}, \quad \forall k \in [0 \dots N-1], \tag{8}$$

- the power converter operates within its limits,

$$-P_{\text{pc,max}} \le P_{\text{bat}}(k) \le P_{\text{pc,max}}, \quad \forall k \in [0 \dots N-1], \tag{9}$$

- the peak power for each month is correctly evaluated ahead of minimization,

$$P_{\text{peak}}(l) \ge P_{\text{grid,max}}(k), \forall k \in \text{month } l \tag{10}$$

- the total investment does not exceed the limit determined by the user,

$$J_{\text{inv}} \le J_{\text{inv,max}} \tag{11}$$

- the investment is paid off within the set number of years,

$$J_{\text{no,inv}} - J_{\text{yes,inv}} \ge \frac{J_{\text{inv}}}{n_{\text{payoff}}} + J_{\text{ym}}. \tag{12}$$

The variable $J_{\text{no,inv}}$ is the cost of the energy exchange with the grid for the case of no investment performed, and DoD is the allowed depth of the battery system discharge.

Upon constructing and solving the LP with cost (4) and constraints (7) – (12), the results are saved and transferred to the next iteration.

Efficiency and degradation iteration

After solving the initial iteration, the efficiency of the BESS and the degradation of the battery pack can be introduced. Since the loss functions are linear at k only if $P_{\text{bat}}(k)$ does not change its sign, a new auxiliary variable $CoD(k)$ is introduced, which determines if the battery charges or discharges at k: $CoD(k)=1$ while charging, and $CoD(k)=-1$ while discharging. After the initial iteration it is calculated as:

$$CoD^0(k) = \begin{cases} 1 \text{ when } \operatorname{sign}\left(P_{\text{bat}}^0(k)\right) = 0 \\ \operatorname{sign}\left(P_{\text{bat}}^0(k)\right) \text{ otherwise.} \end{cases} \tag{13}$$

where $CoD^0(k)=1$ if the battery was neither charged nor discharged. In further iterations enumerated with i the (dis)charging power $P_{\text{bat}}(k)$ should be able to change the sign, and this is ensured by changing $CoD(k)$ from 1 to –1 when $P_{bat}(k)$ changes from positive value to zero, and from –1 to 1 when $P_{bat}(k)$ changes from negative value to zero:

$$CoD^i(k) = 2 \operatorname{sign}\left(P_{\text{bat}}^{i-1}(k)\right) - CoD^{i-1}(k). \tag{14}$$

With the variable determining the direction of the power flow to/from the battery, the efficiency of the BESS at timestamp k, $\eta(k)$ can be expressed as:

$$\eta(k) = \max(0, \eta_{\text{ch}} CoD(k)) - \min\left(0, \frac{1}{\eta_{\text{dch}}} CoD(k)\right), \tag{15}$$

where η_{ch} and η_{dch} are charging and discharging efficiencies. The state of charge of the battery can now be expressed with:

$$SoE(k+1) = SoE(k) + \eta(k) P_{\text{bat}}(k) T_s. \tag{16}$$

The cost of the battery degradation is expressed per unit of energy that goes through it, and it is calculated as:

$$c_{\text{deg}} = \frac{c_{\text{bat}}}{2 n_{\text{cyc}} DoD}, \tag{17}$$

where n_{cyc} is the number of cycles that the battery pack can go through without significantly reducing its capacity. With the degradation costs defined, the costs of the annual maintenance are now calculated as:

$$J_{\text{ym}} = c_{\text{deg}} T_s \sum_{k=0}^{N-1} CoD(k)\eta(k)P_{\text{bat}}(k) + \frac{c_{\text{pc}}}{n_{\text{pc}}} P_{\text{pc,max}} + \frac{c_{PV}}{n_{PV}} P_{PV,\text{peak},ref}\alpha_{PV}. \quad (18)$$

Due to the new definitions of $SoE(k)$ and J_{ym}, the constraints (7), (8) and (12) are updated in the corresponding LP. Furthermore, a new set of constraints is introduced. It makes sure that the (dis)charging power of the battery does not change its sign:

$$\begin{cases} P_{\text{bat}}(k) \geq 0 \text{ when } CoD(k) = 1, \\ P_{\text{bat}}(k) \leq 0 \text{ when } CoD(k) = -1. \end{cases} \quad (19)$$

Feed-in price iterations

So far, the price for the energy exchanged with the utility grid was the same regardless of the sign. For example, if the energy is fed into the grid due to high PV production, the price for it was the same as for buying the energy. However, feed-in prices are normally significantly lower than buying prices. Therefore, a new auxiliary variable $BoS(k)$, which determines whether the energy is bought or sold at timestamp k, is introduced: $BoS(k)=1$ when buying the energy, and $BoS(k)=-1$ when selling the energy. After the initial iteration it is calculated as:

$$BoS^0(k) = \begin{cases} 1, \text{when sign}\left(P_{\text{grid}}^0(k)\right) = 0 \\ \text{sign}\left(P_{\text{grid}}^0(k)\right) \text{ otherwise} \end{cases}, \quad (20)$$

where $BoS^0(k)=1$ if the energy is neither bought nor sold. In further iterations the power exchanged with the grid $P_{\text{grid}}(k)$ should be able to change the sign, and this is ensured by changing $BoS(k)$ from 1 to –1 when $P_{\text{grid}}(k)$ changes from positive value to zero, and from –1 to 1 when $P_{\text{grid}}(k)$ changes from negative value to zero:

$$BoS^i(k) = 2\,\text{sign}\left(P_{\text{grid}}^{i-1}(k)\right) - BoS^{i-1}(k). \quad (21)$$

Therefore, the price of energy exchange with the grid, $c_{\text{el}}(k)$, can be defined depending on $BoS(k)$:

$$c_{\text{el}}(k) = \max\left(0, c_{\text{grid}} BoS(k)\right) - \min\left(0, c_{\text{feed}} BoS(k)\right), \quad (22)$$

where c_{feed} is the feed-in price of the electrical energy. With the newly defined energy price, the cost of energy exchange with the grid, equation (4), now becomes:

$$J_{\text{yes,inv}} = \sum_{k=0}^{N-1} c_{\text{el}}(k) P_{\text{grid}}(k) T_s + c_{\text{peak}} \sum_{l=1}^{12} P_{\text{peak}}(l). \quad (23)$$

Due to the new definitions of $J_{\text{yes,inv}}$ the cost function of the LP and constraint (12) are updated. Furthermore, a new set of constraints is introduced. It makes sure that the power exchange with the utility grid does not change its sign,

$$\begin{cases} P_{\text{grid}}(k) \geq 0 \text{ when } BoS(k) = 1, \\ P_{\text{grid}}(k) \leq 0 \text{ when } BoS(k) = -1. \end{cases} \quad (24)$$

There is no guarantee on feasibility for the newly formed LP. Because of the lowered feed-in price the revenue from selling the energy will be lowered which means a lower investment possible, and with fixed directions of power flows between the consumer and the grid there might be no feasible solution. Therefore, the feed-in price c_{feed} is gradually changed until the proper solution is found.

Firstly, the LP is formulated with the proper feed-in price c_{feed}. If the solution is feasible then the procedure proceeds to the converging iterations. On the other hand, if the solution of this LP is infeasible, the feed-in price is artificially brought halfway back to the buying price c_{grid} as $c_{\text{feed,artificial}}=(c_{\text{grid}}+c_{\text{feed}})/2$. If the solution is infeasible again, the halving of the interval between current feed-in price and the buying price is repeated until the feasible solution is found. After the feasible solution is found, the LP is formulated again with the proper feed-in price. This time, if the solution is infeasible, the new artificial feed-in price is brought halfway back to the feed-in price that resulted in feasible solution for the last iteration: $c_{\text{feed,artificial}}=c_{\text{feed}}^{i-1}+c_{\text{feed}})/2$. If the solution is infeasible again, the procedure of interval halving is repeated until a feasible solution is obtained.

Converging iterations

The last set of iterations is carried out until convergence. The LP problems have the same construction as the feed-in price iterations. The only difference is the feed-in price that is now fixed at the proper value. Every time the LP problem is solved auxiliary variables CoD and BoS are updated. Also, every time the LP is solved, the value of its cost function is compared with the minimal value so far. If it is less than the minimum so far, the procedure continues with further iterations. However, if the value of the cost function is greater than the minimum so far, the counter for convergence increases by 1. When the counter reaches the setpoint number the procedure ends, and the optimal result is the one with the minimum value of the cost function.

3. Results

The site used for showcasing the results of the procedure is Bračak manor in Croatia. It is a recently refurbished manor used as an office space. Its power consumption over a one-year horizon is shown in Figure 1. The length of the prediction horizon in this case is N = 35136, since 2018 was a leap year, and the sampling time was T_s = 15 min.

The canopy built at the site where the PV array was installed has south-west orientation, and it is inclined by 15°. With such an orientation and inclination angles the possible PV production with the peak power of 3 kWp has the profile shown in Figure 1.

The lifetime of the PV system is 25 years, which is a typical warranty time for solar panels. The results presented were obtained for two different prices of the PV system: 1050 €/kWp, and 420 €/kWp which is the original price with 60% subsidies. Other parameters are:

- Number of cycles (n_{cyc}): 2000
- Depth of discharge (DoD): 0.8 (80%)
- Discharging efficiency (η_{dch}): 0.9 (90%)
- Charging efficiency (η_{ch}): 0.9 (90%)
- Lifetime of power converter (n_{pc}): 25 years
- Price of the new battery pack (c_{bat}): 770 €/kWh
- Price of the new power converter (c_{pc}): 660 €/kW

The results are presented in Tables 1, 2, and 3.

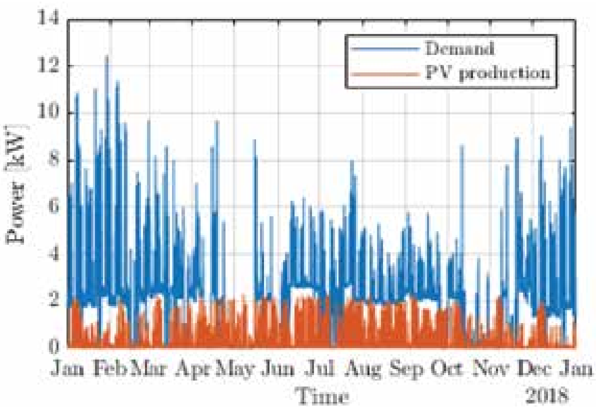

Figure 1. Electric power demand profile P_{dem} at Bračak site for year 2018, and the nominal (α_{PV}=1) PV production profile.

Table 1. Optimal PV + BESS sizes for the Bračak site for the investment payoff period, n_{payoff}, of 10 years.

PV system subsidies	0%	60%
Battery capacity (SoE_{max}) [kWh]	0.00	2.60
Power converter power ($P_{pc,max}$) [kW]	0.00	1.91
PV system peak power ($P_{PV,peak}$) [kWp]	0.00	9.97

Table 2. Optimal PV + BESS sizes for the Bračak site for the investment payoff period, n_{payoff}, of 15 years.

PV system subsidies	0%	60%
Battery capacity (SoE_{max}) [kWh]	0.00	3.23
Power converter power ($P_{pc,max}$) [kW]	0.00	1.65
PV system peak power ($P_{PV,peak}$) [kWp]	10.00	10.00

Table 3. Optimal PV + BESS sizes for the Bračak site for the investment payoff period, n_{payoff}, of 20 years.

PV system subsidies	0%	60%
Battery capacity (SoE_{max}) [kWh]	0.00	4.93
Power converter power ($P_{pc,max}$) [kW]	0.00	3.17
PV system peak power ($P_{PV,peak}$) [kWp]	10.00	10.00

4. Conclusion

In this paper a procedure to find optimal sizing parameters of a PV system in combination with a BESS for a particular consumer is outlined. Optimal parameters are the peak power of the PV system, and battery energy capacity and power converter rated power of the BESS. Furthermore, the procedure also gives optimal charging and discharging powers at each time step for the whole horizon. The procedure uses pre-recorded energy consumption of the consumer and possible PV power production. The backbone of the procedure is an SLP method that replaces the large and memory-intensive LP problem which guarantees to find the global optimum. The paper contains a detailed explanation of the procedure and the formulation of the subsequent LP problems with their constraints and cost functions and gives experimental results for a real consumer.

Acknowledgment

This work was supported by the Interreg CENTRAL EUROPE Programme, funded under the European Regional Development Fund, through the project Integration and smart management of energy storages at historical urban sites (Store4HUC, https://www.interreg-central.eu/Store4HUC).

References

[1.] Aneke, M. and Wang, M. (2016). Energy Storage Technologies and Real Life Applications – A state of the art review. Applied Energy, 179, 350-377.

[2] Sharma, V., Haque, M. H., and Aziz, S. M. (2019). Annual Electricity Cost Minimization for South Australian Dwellings through Optimal Battery Sizing. In Proc. IEEE Milan PowerTech, 1-6.

[3] Farahmand, M. Z., Nazari, M. E. and Shamlou, S. (2017). Optimal sizing of an autonomous hybrid PV-wind system considering battery and diesel generator. In Proc. Iranian Conference on Electrical Engineering (ICEE), 1048–1053.

[4] Mahesh, A. and Sandhu, K. S. (2016). Optimal sizing of a PV/Wind hybrid system using pigeon inspired optimization. In Proc. IEEE 7th Power India International Conference (PIICON), 1-6.

[5] Rukavina, F. and Vašak, M. (2020). Optimal parameterization of a PV and a battery system add-on for a consumer. In Proc. IEEE 11th International Symposium on Power Electronics for Distributed Generation Systems (PEDG), 619-622.

[6] Store4HUC project, Interreg Central Europe. (2019). Available at: www.interreg-central.eu/Store4HUC

Hrvoje Novak [1,2], *Vinko Lešić* [1], *Mario Vašak* [1]

Coordinated Energy Management of the Electric Railway Traction System: Croatian Railways Case Study

[1] University of Zagreb, Faculty of Electrical Engineering and Computing, Department of Control and Computer Engineering, Laboratory for Renewable Energy Systems, Unska 3, 10000 Zagreb, Croatia,
[2] Innovation Centre Nikola Tesla, Unska 3, 10000 Zagreb, Croatia

Abstract

A railway energy management system based on hierarchical coordination of electric traction substation energy flows and on-route trains energy consumption is presented in the paper. The railway system is divided into energy-efficient individual trains energy consumption management as a lower level, and the energy-cost-efficient electric traction substation energy flows management as a higher level. The levels are coordinated through parametric hierarchical model predictive control with the main goal of additionally decreasing the operational costs of the overall system. Through interactions with the power grid at the higher level, the system can provide ancillary services and respond to various grid requests. At the same time, lower level trains driving profiles are adjusted to attain the minimum cost of system operation with timetables and on-route constraints respected. The developed algorithm is verified against a detailed real case study scenario with the presented results showing significant cost and energy consumption reductions.

Keywords: *train traction energy consumption, electric traction substation energy flows, energy management, hierarchical model predictive control.*

1. Introduction

In order to cope with the rise in transport demand and recent increase of railway activity [1], electric railway traction systems are a promising area for the implementation of advanced energy management strategies with the goal of increasing energy efficiency and reduction of CO_2 emissions (emphasized in the European Union climate and energy targets for 2030 [2]). With the integration of driver advisory systems, advanced energy meters, four-quadrant drives and various energy storage technologies, railway systems are transforming through smart control systems into active participants in the power grid.

A significant research focus of railway system energy efficiency is put on: (i) reducing the energy consumption of an individual train as in [3] and, more recently, on (ii) better utilization of regenerative braking energy, either by timetables optimization [4], or by introduction and implementation of different energy storage systems [5]. Energy-efficient train driving methods minimize energy consumption during train travel between adjacent stations while respecting the timetables, on-route restrictions (speed limits, train traction force boundaries etc.) and passengers' comfort, with savings of up to 30% reported in [4]. Optimization of timetables, so that multiple trains acceleration and braking intervals are synchronized, shows possible energy consumption reductions by up to 29%, with an extensive survey presented in [4]. Combination of multiple energy storage systems (batteries, supercapacitors and flywheels) introduces an additional energy savings potential by up to 30% [5]. Integrated approaches, which jointly optimize the timetable and trains driving profiles, show improved performance since they take into account the minimization of the tractive energy consumption of each train while maximizing the utilization of regenerative energy between multiple trains [6]. The listed railway system energy efficiency approaches exclude the power grid perspective. The focus is instead put solely on the processes and subsystems of the railway system. The possible benefits of railway system active interaction with the future electricity grids show the railway system ability to participate in energy markets, offer ancillary services to the power grid operator [7] and integrate renewable energy sources [8]. However, this is done without considering the optimization of timetables or traction profiles, thus ignoring the significant potential in their rearrangement.

In this paper, the railway system is considered through the coordination of the on-route trains energy consumption level and the electric traction substation (ETS) energy flows management level with the goal of increasing energy efficiency, decreasing operational costs and enabling the integration of railways into smart electricity grids. The algorithm for hierarchical coordination is developed and presented in [9] together with a case studydesigned for the verification of the developed control system within a realistic scenario taken from Croatian Railways.

The paper is organized as follows. Problem definitions at both levels are presented in Section 2 together with the concept of hierarchical coordination between the levels. The realistic case study scenario is described in detail in Section 3 together with the corresponding results presented in Section 4. The conclusions are given in Section 5.

2. Hierarchical model predictive control for coordinated energy management

Optimization problems for both on-route trains energy consumption (lower) and ETS energy flows management (higher) levels are described hereinafter.

Lower hierarchical level

The method for energy consumption minimization of a single train traveling between two stations was initially described in [10, 11] where explicit constrained finite-time optimal control of piecewise affine systems is employed to calculate the optimal traction force control law. The energy-efficient train driving control problem aims at finding the train traction/braking force that minimizes the mechanical energy consumption used for train traction while reaching the next station at the allotted time and continuously respecting all the physical constraints imposed on train speed, traversed path and traction force along the rail path.

Higher hierarchical level

At the higher, energy flows optimization level, the model predictive control (MPC) problem is formulated with a linear cost function for the economically optimal energy flows [9]. A single ETS is observed from the point of balancing energy flows between the accelerating and decelerating trains, the energy storage system and a connection to the utility grid with variable energy prices and various demands from the utility grid operator. Energy flows optimization results in optimal charging/discharging profiles for storage components that guarantee the optimal economic cost on the prediction horizon while taking into account the current state-of-charge of the energy storages, predicted trains consumption profile, volatile electricity price profile representing the economic criterion of the utility grid, and technical constraints in system components. The HHL problem is reformulated as a multi-parametric MPC problem with the parameters set obtained from the LHL.

Hierarchical coordination for energy management

Hierarchical coordination between the LHL and HHL is performed through revisiting of both control levels with the goal of improving the initial energy-optimal LHL solution for individual trains with respect to the HHL cost for energy exchange, thus transforming it into a global economically optimal solution for the traction substation. The iterative coordination scheme is depicted in Fig. 1, executed until the LHL solution converges

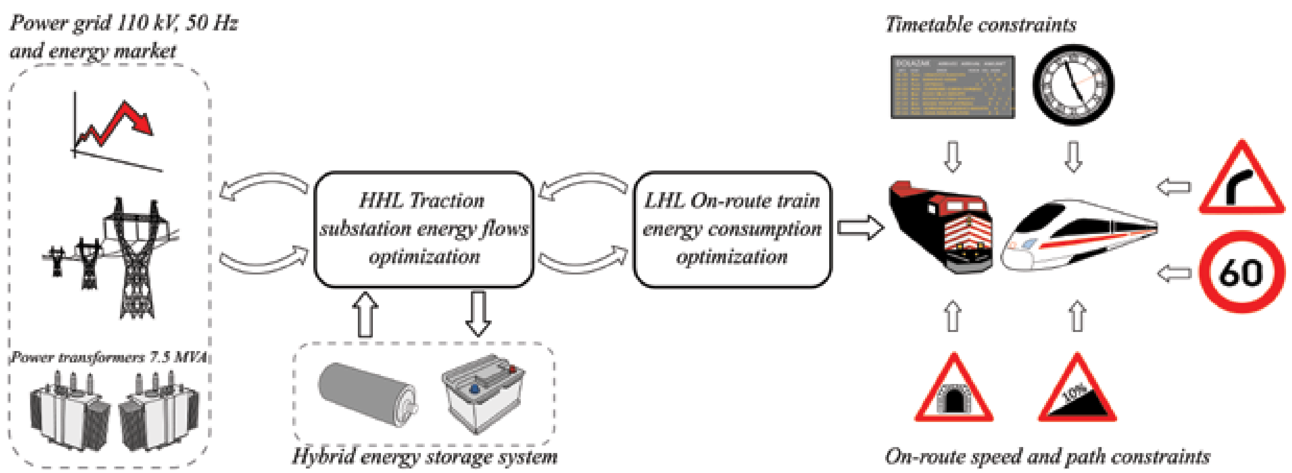

Fig. 1. Scheme and information flow of hierarchical coordination between LHL and HHL optimizations.

with respect to the global criteria under the given constraints, i.e. when the train traction force energy-optimal profile is shifted to the price-optimal profile. A detailed description and mathematical formulation of the hierarchical coordination algorithm is presented in [9].

The modularity and hierarchical structure of the presented algorithm keeps the considered subsystems operation apart since they are often required to remain infrastructurally and technologically independent, but also usually legally separated to infrastructure companies for operating power supply and different transportation companies for operating the trains. Due to the modular structure of the algorithm, the levels are able to operate independently when e.g. the train operation at the lower level cannot be changed. It is also possible to extend the proposed algorithm with new levels, e.g. for the simultaneous coordination of multiple traction substations so that a longer rail segment of the infrastructure operator is considered.

3. Case study simulation scenario

The case study is based on actual trains, time schedules and rail route configurations. The trains time-schedule and rail route configuration are taken from the railway section of Corridor X of Croatian Railways Infrastructure in Slavonia region (eastern Croatia) [12]. A traction segment of ~56 km (between the two neutral sections) supplied from ETS Andrijevci was selected. It includes 10 passenger stations, has small to no track gradient and no curves or tunnels. The considered rail path is depicted in Fig. 2 with the corresponding passenger stations locations. Travel distances and times are presented in [9].

The considered train configuration is the low-floor electromotive train (EMT) for the urban and commuter operation manufactured by Končar - Electric Vehicles Inc. [13]. The EMT is designed as a low-floor four-part train with a total length of 75 m, built for rails electrified with catenary power supply of 25 kV voltage and 50 Hz frequency, with a maximum speed of 160 km/h. The detailed Končar EMT parameters can be found in [9].

The connection to the utility grid is made via two 110/25 kV transformers of 7.5 MVA power each. The transformers have the ability to return energy back to the utility grid (with imposed amount limit set to 1 MW) which offers a possibility for interaction with the power grid and better utilization of excessive regenerative and/or stored energy. The considered hourly varying prices for energy exchange are based on European Power Exchange prices (EPEX [14]), which are available one day ahead.

The energy storage system is modeled as a joint operation of battery energy storage system and a supercapacitor. Selection of the supercapacitor is justified for collecting the regenerative braking energy with large number of charging/discharging cycles, due to its large power density, while battery storage is selected with the aim of collecting larger amounts of energy during longer periods of time, due to the battery high energy density. The considered energy storage system parameters are based on commercially available storage systems listed in [9].

4. Simulation results

Traveling through ETS Andrijevci supply area lasts around 60 minutes (including 1 minute stops in all passenger stations) according to the Croatian Railways timetable for the rail path length of 60.7 km between stations Slobodnica and Ivankovo. The calculated

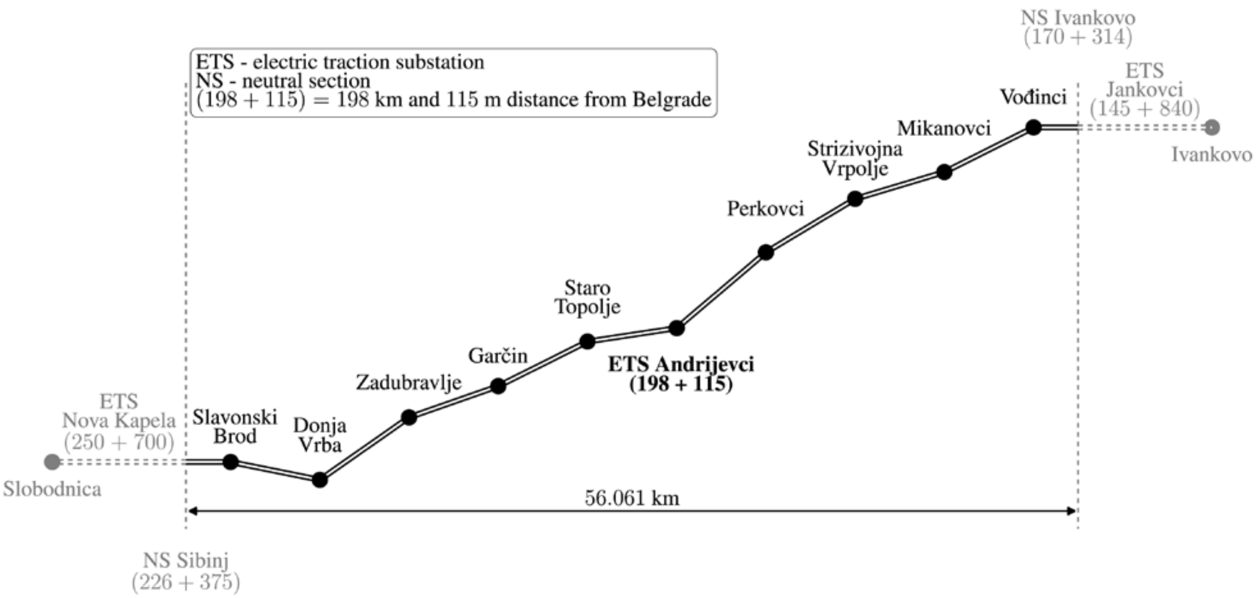

Fig. 2. Croatian Railways Corridor X section area supplied from ETS Andrijevci with the corresponding passenger stations.

energy-optimal train traction force profile is presented in Fig. 3 together with the corresponding travel speed and traversed path profiles.

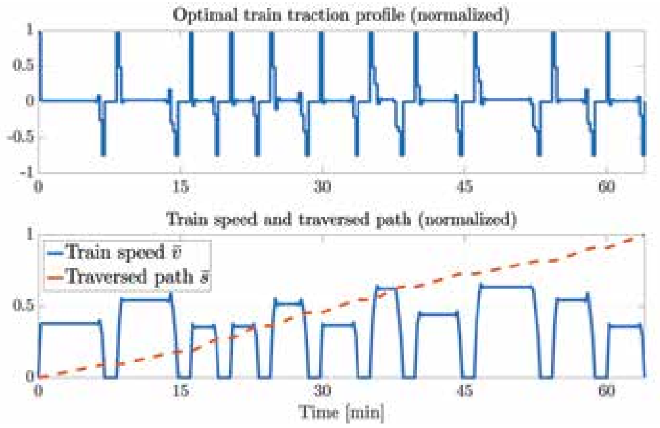

Fig. 3. Energy-optimal train traction force, speed and traversed path profiles while traveling from Slobodnica to Ivankovo.

After the initial results are obtained from the LHL, the energy-optimal train travel consumption profile is created for a train traveling through the ETS Andrijevci supply area. To simulate the Croatian railways timetable for the considered ETS Andrijevci area for one day, the created travel profiles from Fig. 3 are stacked in time with all the passenger trains considered identical.

The HHL control system operation is simulated during a daily system operation according to the Croatian Railways timetable together with volatile EPEX prices and a prediction horizon of 24 h. Simulation scenario results are depicted in Fig 4 and comprise of: (i) energy exchange price profile, (ii) ETS power flows (summed trains energy consumption/production), (iii) energy exchanged with the utility grid and (iv) energy storage state of charge for both energy storage components.

The hierarchical coordination algorithm is simulated for the period between 13:00 and 14:00 with all together 13 trains supplied from ETS Andrijevci at some point during the one-hour period, according to the timetable.

From the results presented in Figures 5 and 6, the following is observed: (i) the coordination between the control levels reduces the amount of energy that is being unused, i.e. dissipated in the resistors (shown with the red line in the first plots of both figures), (ii) the peaks of produced regenerative energy are reduced as the regenerative energy production from a single train is being distributed towards other trains (shown with the

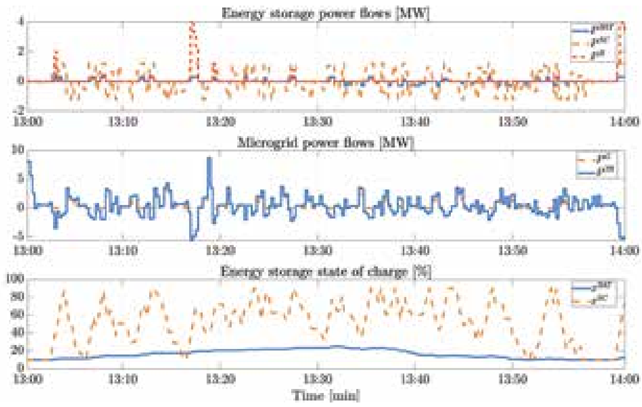

Fig. 5. One-hour system behavior without coordination.

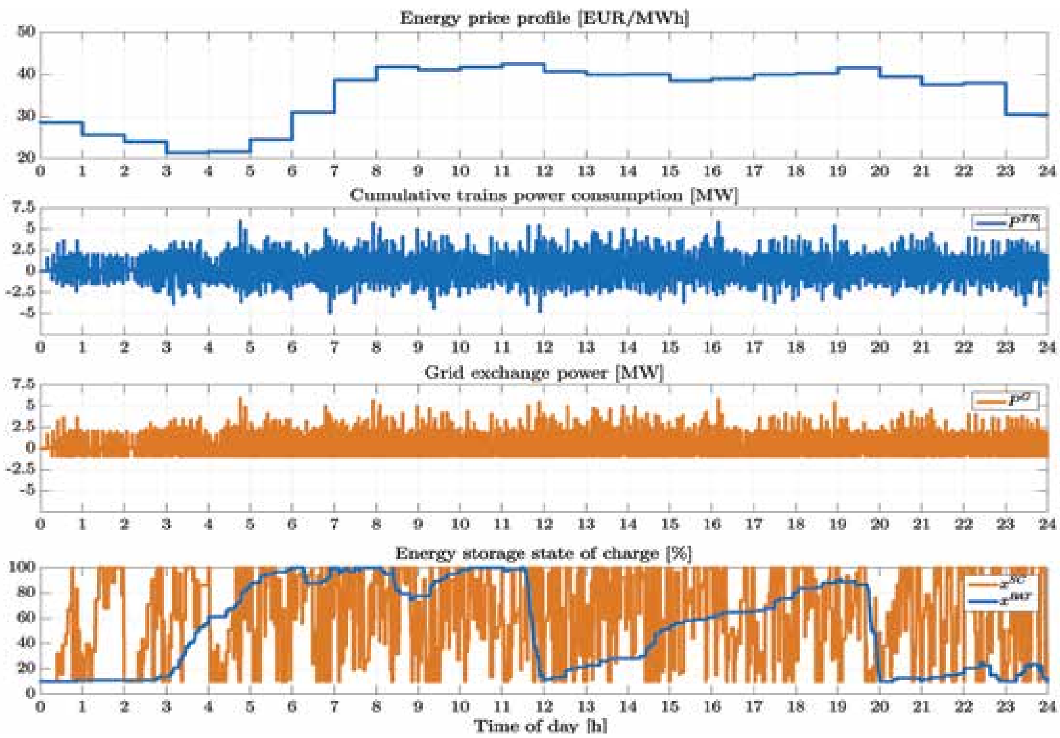

Fig. 4. Daily power flows for system operation with only higher level MPC installed and grid receptiveness of -1 MW

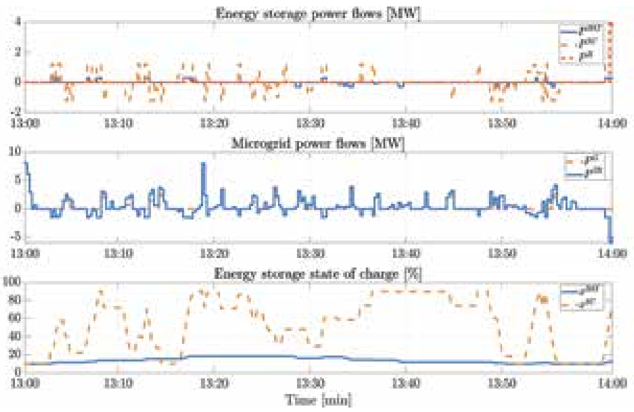

Fig. 6. One-hour system behavior with coordination.

blue lines in the middle plots of both figures) and (iii) the use of the energy storage systems is reduced since their operation causes energy losses due to energy efficiency of the storage technologies (shown with the red and orange lines in the first and last plots of the figures).

The power consumption of individual trains during this one-hour simulation period is presented in Fig. 7, individually for four trains that are supplied during most of the one-hour period from the considered ETS, and cumulatively for the remaining 9 trains. The neighboring trains exchange energy and cooperate in order to reduce system operation costs. Such energy exchange between the trains can be seen when more trains are in braking and therefore generate a large amount of energy that is then consumed by other trains currently supplied from the same ETS, and now deviate from their initial traction profiles in order to consume this energy. Although these trains then operate with a suboptimal traction profile and actually consume more energy, the system benefits from this interaction between trains since most of the regenerative braking energy would be dissipated if the trains would not be coordinated. This behavior can be seen in Fig. 7 where e.g. Train 1 speeds up at 13:03 to consume the energy generated by the remaining trains and reduces the cumulative regenerative energy peak (subplot 5), or where trains 3 and 4 brake early at 13:15 and 13:17, respectively, to shift their consumption profiles and reduce the overall regenerative energy production from 13:17 to 13:18 (subplot 5). Although the traction profiles of the trains change, the schedule is maintained, and operational constraints are respected.

Different variations are introduced to the initial simulation set-up, with corresponding cost and energy consumption reductions compared and the results presented in Fig. 8. Cost and energy reduction quantities in all cases are obtained through comparison with the costs and energy consumption of system operation without the HHL control and with trains driven in the energy-optimal way.

The results obtained via solely MPC applied to a higher level control with energy-optimal traction profiles applied for individual trains, but without coordination, are then compared with the baseline case and the results achieved with coordination. The results obtained show that the energy consumptions reductions reach up to 40%

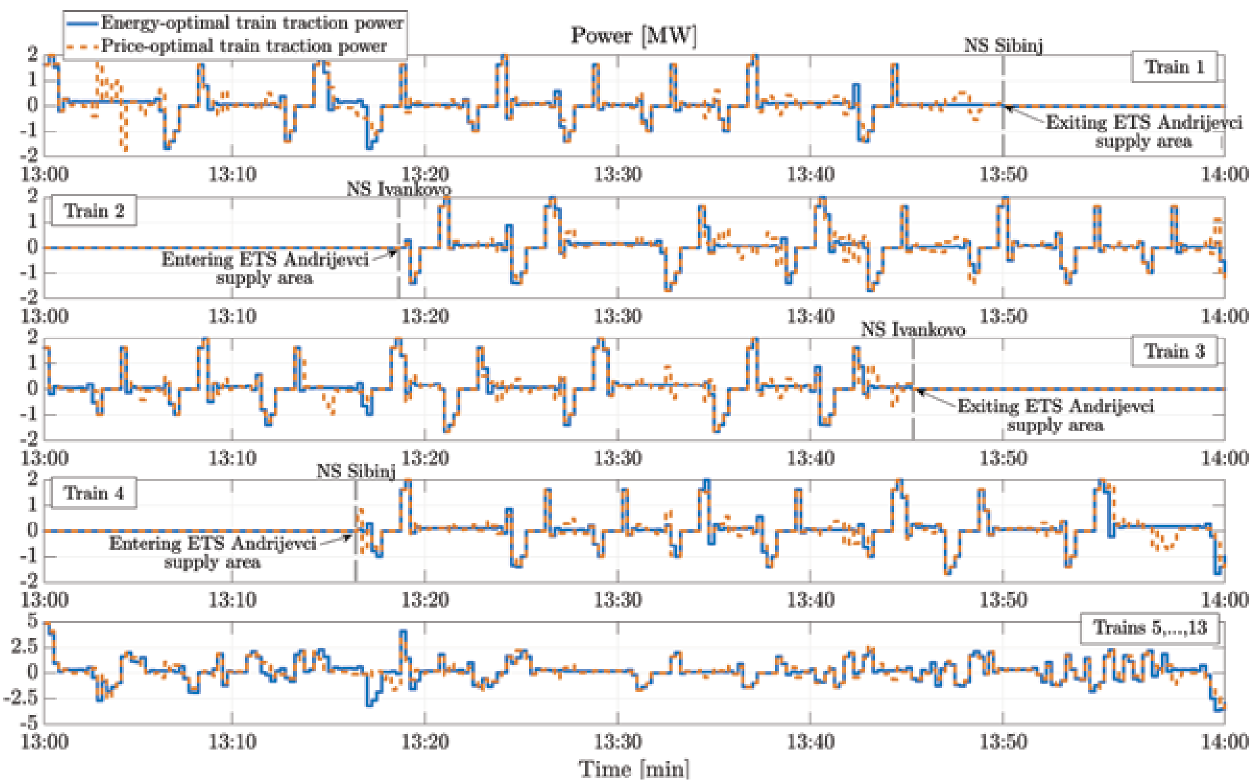

Fig. 7. Power consumption profiles of all trains supplied from ETS Andrijevci, before and after hierarchical coordination, for a one-hour system operation

while the costs are reduced up to 45%, as presented in Fig. 8.

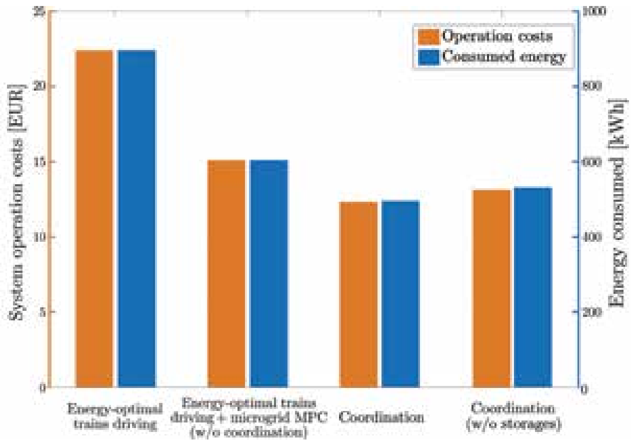

Fig. 8. Energy consumption and system operation costs for different control setups for the one-hour system operation

An additional simulation case was added to the setup, in order to investigate system operation without energy storage systems implemented and with coordination between the levels. From the results presented in Fig. 8 it is observed that the software-based coordination at the lower level can eliminate the need for storages, since the cost reductions are only slightly decreased when no energy storage systems are installed in the system. Although such control system setup does not provide the best possible results, it also does not require large financial investments for the installation of energy storage systems. It is therefore closer to the implementation on actual railway systems and shows an important advantage of the analyzed coordination.

5. Conclusion

In this paper, an algorithm for energy- and cost-efficient control of the electric railway system is presented. The algorithm is based on the hierarchical coordination of the electric traction substation energy flows control level (higher) and individual trains traction energy consumption control level (lower) and is verified by means of a detailed case study. The results presented show promising savings possibilities, which reach up to 45% cost reduction and 40% reduction of energy consumed compared to the non-coordinated case in which trains are optimally driven.

Each level of the presented modular control system contributes to the increase of savings, while keeping the possible implementations of the control system flexible and adaptable to various railway system configurations. Through interactions with the power grid, the system is transformed from a passive energy consumer to a proactive user able of responding to various grid demands as well as providing services to the power grid operator.

References

[1] International Energy Agency and International Union of Railways, “Railway Handbook 2017 - Energy Consumption and CO_2 Emissions.”

[2] European Commission, “A policy framework for climate and energy in the period from 2020 to 2030.”

[3] Y. Wang, B. Ning, F. Cao, B. De Schutter, and T. van den Boom, “A survey on optimal trajectory planning for train operations,” in Proceedings of 2011 IEEE International Conference on Service Operations, Logistics and Informatics, 2011, pp. 589–594

[4] X. Yang, X. Li, B. Ning, and T. Tang, “A survey on energy-efficient train operation for urban rail transit,” IEEE Transactions on Intelligent Transportation Systems, vol. 17, no. 1, pp. 2–13, 2016

[5] T. Ratniyomchai, S. Hillmansen, and P. Tricoli, “Recent developments and applications of energy storage devices in electrified railways,” IET Electrical Systems in Transportation, vol. 4, no. 1, pp. 9–20, 2014

[6] X. Sun, H. Lu, and H. Dong, “Energy-efficient train control by multi-train dynamic cooperation,” IEEE Transactions on Intelligent Transportation Systems, vol. 18, no. 11, pp. 3114–3121, 2017

[7] E. Pilo de la Fuente, S. Mazumder, and I. Gonzalez Franco, “Railway electrical smart grids: An introduction to next-generation railway power systems and their operation.” IEEE Electrification Magazine, vol. 2, no. 3, pp. 49–55, 2014

[8] P. Pankovits, J. Pouget, B. Robyns, F. Delhaye, and S. Brisset, “Towards railway-smartgrid: Energy management optimization for hybrid railway power substations,” in Innovative Smart Grid Technologies Conference Europe (ISGT-Europe), 2014 IEEE PES, 2014

[9] H. Novak, V. Lešić and M. Vašak, "Hierarchical model predictive control for coordinated electric railway traction system energy management," in IEEE Transactions on Intelligent Transportation Systems, vol. 20, no. 7, pp. 2715-2727, July 2019

[10] M. Vašak, M. Baotić, N. Perić, and M. Bago, “Optimal rail route energy management under constraints and fixed arrival time,” in Proceedings of the European Control Conference 2009, 2009, pp. 2972–2977

[11] H. Novak, V. Lešić and M. Vašak, "Energy-efficient model predictive train traction control with incorporated traction system efficiency," in IEEE Transactions on Intelligent Transportation Systems (Early Access), 2021.

[12] HŽ Infrastruktura Ltd., “Network Statement 2015,” 2014

[13] Končar Electric Vehicles Inc., “Electric Multiple Units,” http://www.koncar-kev.hr/products_and_services/electric_multiple_units

[14] EPEX SPOT. European Power Exchange Electricity Index. [Online]. Available: http://www.epexspot.com

Vinko Lešić[1], *Hrvoje Novak*[1,2], *Marko Ratković*[2]

Rapid Plant Development Modelling System for Predictive Agriculture

[1] University of Zagreb, Faculty of Electrical Engineering and Computing, Department of Control and Computer Engineering, Laboratory for Renewable Energy Systems, Unska 3, 10000 Zagreb, Croatia
[2] Innovation Centre Nikola Tesla, Unska 3, 10000 Zagreb, Croatia

Abstract

Actual and upcoming climate changes will evidently have the largest impact on agriculture crops cultivation in terms of reduced harvest, increased costs, and necessary deviation from traditional farming. The aggravating factor for the successful applications of precision and predictive agriculture is the lack of big data due to slow, year-round cycles of crops, as a prerequisite for further analysis and modelling. The goal of our proposed system is to enable rapid collection of data with respect to various climate conditions, which are artificially created and permuted in the encapsulated design and correlated with plant development identifiers. The design is equipped with a large number of sensors and connected to the central database in a computer cloud, which enables the interconnection and coordination of multiple geographically distributed devices and related experiments. This accumulated data is exploited to develop mathematical models of wheat at different growth stages by applying the concepts of artificial intelligence and to utilize them to predict crop development and harvest. The paper focuses on a system concept to gather data for future models to be used publicly and interactively through a portal for predicting plant development under real and hypothetical climate conditions.

Keywords: *plant growth encapsulated design, rapid plant development modelling; IoT, big data, artificial intelligence, predictive agriculture.*

1. Introduction

Artificial intelligence (AI) today is significantly focused on increasing the efficiency of different sectors and reducing negative impacts on the environment. The agriculture sector started adopting the AI only recently, following the development of Internet of Things (IoT) as distributed networks of sensors and other devices [1] that enabled precision agriculture and the formation of large datasets [2]. The number of IoT devices in agriculture was projected to increase from 30 million in 2015 to 75 million in 2020 [3] and to offer significant precision farming opportunities such as: crop monitoring, disease detection, storage optimization, treatment optimization, irrigation and weeding [4, 5]. Successful examples of precision agriculture analytics include crop prediction by fruit counting or estimation from crop images with different spectra with 70-90% reliability of estimation accuracy [6], or modelling and forecasting of corn yield by neural networks depending on soil treatment [7]. A wider application of these methods is still in its infancy, as research began only a few years ago, mainly out of concern for climate change. The biggest aggravating factor for the successful application of AI is the lack of large amounts of data as a prerequisite for further analysis and modelling. Due to slow, year-round cycles, and the distinct specificity of individual locations (soil and weather conditions), it is not possible to promptly create a significant database of historical data. In addition, it is necessary to install a large number of sensors on different fields, which is one of the most propulsive areas of modern agriculture [8]. Moreover, climate changes are one of the most expressed aggravating factors for obtaining the relevant datasets.

The "big data" issue is addressed here by creating specially designed bioreactors that serve as rapid plant model identification systems of multiple simultaneous climate zones, supported by autonomous real-time data acquisition and archiving. Instead of the usual observed annual life cycles in nature, the system introduces equipment for rapid, simultaneous implementation of a number of different experiments in a climate-encapsulated system with control loops of light, temperature, humidity, pH and nutrient profiles, with an extensive network of sensors and with the help of multi-spectral cameras. The equipment is supported by software in the form of an autonomous storage of identifiers in a central database. For the exemplary case of the wheat, a single encapsulated design enables 8-12 simultaneous plant groups, each one as individual field emulation, capable of squeezing up to three yield cycles in a single year, resulting in total with 24-36 harvests per year per device that is the size of a computer server cabinet.

With a significant amount of historical data available, mathematical models of several different stages of wheat crop development are developed using AI (artificial neural networks, genetic algorithms) with respect to different, artificially created and permuted, microclimate conditions correlated with identified plant growth and development indicators at different stages.

The paper is a concise version of [11], organized as follows. Overall methodology of the approach is presented in Section 2. Encapsulated design and basic features are described in Section 3 while the architecture of the supporting IT system is described in Section 4. The AI plant development models are outlined in Section 5 and the conclusions are presented in Section 6.

2. Rapid plant modelling system methodology

The proposed methodology utilises the developed encapsulated design (apparatus) for accelerated experiments of plant growth in an isolated environment with autonomous permutation of artificial climatic conditions (light profile, temperature, humidity, airflow, pH and nutrient level) and archiving plant growth and development indicators collected by different sensors and multi-spectral cameras. The apparatus, i.e. the prototype of the system, implies constructional, assembly and electronic preconditions, and corresponding control loops to achieve the desired stated conditions in real-time and at the same time to regulate several different climatic conditions in an isolated environment.

The constructional prerequisite of the system ensures isolation from external conditions and enables a spatially compact design suitable for separating several different climatic conditions. The isolated environment also allows the simulation of conditions that are not yet present in the considered climates but are expected to occur under the influence of climate changes. The prerequisite includes a system for irrigation and nutrient supply through pumps and tubes to each individual plant, artificial LED lighting of different spectra and a heating and cooling system.

The electronic prerequisite includes electronic support, sensors, and control hardware for the regulation of the mentioned climatic conditions, as well as support for easy adjustment of parameters for future experiments. The implementation of experiments aims to be significantly accelerated by the simultaneous possibility of providing different conditions and the use of cameras and a mesh grid network of sensors with autonomous archiving of data in real time, which is then a suitable starting point for determining correlations between conditions and plant growth through advanced machine learning algorithms.

The proposed methodology aims at isolating plant physiognomy identifiers that are related to the faster or slower plant development at different stages. There are roughly one hundred phenological stages of wheat growth (BBCH scale) [9] and the system shares the data for three generalized ones: i) germination, ii) plant formation and maturation, iii) grain maturation, which are a general approximation for many plants, with the open possibility for the concept to be transferable to other species. Physiological identifiers such as stomatal transpiration, photosynthetic effect, night respiration, intercellular carbon dioxide concentration, evaporation, etc. are associated with physical and more accessible, i.e. measurable, identifiers such as water and nutrient absorption measured by multi-spectral camera, precise growth measurement, images in different spectra in certain modes (day and night), etc. Individual relevant parameters measurable by sensors and correlation with the growth and development of the plant are autonomously archived in real time together with the given climatic conditions in which the plant is located, gradually forming a very large database suitable for determining correlation relationships by advanced machine learning algorithms. Thus obtained, accurate data on isolated and artificially created climatic conditions and consequent plant development are autonomously archived and over time build a large data set of 6 million records collected in 5000 climate scenarios over a period of 2 years, which is suitable for applying algorithms in mathematical modelling and then predicting future plant developments in the coming climate change. The obtained mathematical models will be checked on a separate set of data and with the identification of the reliability of the estimate based on the forecasted conditions to give a prognostic illustration of the expected plant development. To increase the reliability of prediction, the models are classified and reduced to three parts depending on the plant stage: i) germination, ii) plant formation and maturation, iii) grain maturation.

The objectives of the system are as follows:

- develop the apparatus for rapid plant growth data collection, storage, and processing,
- conduct experiments in 5000 climate scenarios over a period of 2 years,
- obtain a relevant dataset of 6 mil. entries for the chosen wheat crop,
- apply machine learning algorithms for 3 different growth stages to obtain various use-case models of wheat crop development,
- structure the dataset and the models to be exploited for prediction of crop maturation, grain moisture and optimisation of pest treatments.

3. Encapsulated design plant growth devices

By being able to control the microclimate environment, the encapsulated design exploits the outdoor environment and further superposes desired artificial environment (temperature, soil humidity, air humidity, photosynthetic lighting, CO_2 and O_2 concentration and aeration) to experiment plant growth and development under different (sometimes extreme) microclimate conditions, collect and analyse the data to build artificial models that are further used for large scale harvesting predictions. The structure of the encapsulated design is shown in Fig. 1 with the upper part intended for plant growth and environment control and electronic support located within the enclosed drawer. It is important to note that within a single device it is possible to achieve four separate microclimatic zones with corresponding sensors and actuators in each zone. The considered devices are based on intelligent, self-sustainable home gardens of Urban Oasis Croatian manufacturer, which was additionally modified by the research team to enable a system for rapid modelling of plant development.

Fig. 1. Encapsulated design plant growth device [11].

The measured microclimate parameters are: i) air temperature, air flow, air humidity, photosynthetic photon flux density and soil moisture. Plant development indicators are the spectral image light intensity (3 bands), leaf area index (estimated), normalized difference vegetation index (NDVI), simple ratio (SR), photochemical reflectance index (PRI) and chlorophyll index (CI).

Climate parameters regulation

Air temperature: temperature control is achieved using temperature sensors, positive temperature coefficient (PTC) ceramic insulated heaters, ventilation system and the influence of the disturbances such as LED lights, solar irradiance through glass cabinet or electronic devices residual heating. The heating element is used in combination with fans to control the air flow.

CO_2 concentration: by cabinet ventilation, the plants have access to the surrounding CO_2 concentration, and photosynthesized oxygen is removed from the encapsulated design. Increased CO_2 concentrations are achieved by putting the devices in a populated environment (faculty offices) where the concentration can reach up to 3000 ppm. There are two modes of operation: night (respiratory) and day (photosynthetic), both regulated with the inflow and outflow of the external air and CO_2 sensors in the individual zones and matching control loops with PI controlled fan speeds.

Lighting: for normal growth, the plants require approximately 500-1500 μmol/m²/s of PPFD, which is the amount of PAR spectrum photons that reach the plant [10]. This correlates with required 200-500 W per m² of LED light power of the PAR spectrum, which is additionally increased to compensate the distance from the light source. Rather than having a multi-kilowatt lighting system, the sunlight is fully exploited by the glass structure of the encapsulated design, and artificial lighting is used to additionally increase the intensity, permute the outside conditions and extend the luminance duration. Artificial lighting is controlled by PI controller of the LED lighting intensity by PWM and a photosensor, individually in all four zones.

Soil moisture and air humidity: water is delivered to the soil by pumps and valves to each of the four zones individually and controlled by corresponding hysteresis controllers based on the information gathered from the electrical conductivity sensors placed in the soil. Valve on/off duration transforms the water flow in the tubes that supply water to the soil from within of the central tower. In the plant area of the encapsulated design, the humidity control loop consists of a humidity sensor, an ultrasonic humidifier and a corresponding fan that distributes the mist into the leaves. The setpoint of 0-100% humidity is achieved by a PI controlled fan speed.

Nutrients: the amount of required nutrient chemicals for plant growth has a significantly slower dynamics than other systems, with a measurable difference occurring after few months with real-time pH embedded sensors grade. Therefore, the soil is preconditioned prior to conducting the experiments in a laboratory environment and with highly accurate pH level sensors.

An exemplary established microclimate in the four zones of the device is shown in Fig. 2 as time-responses

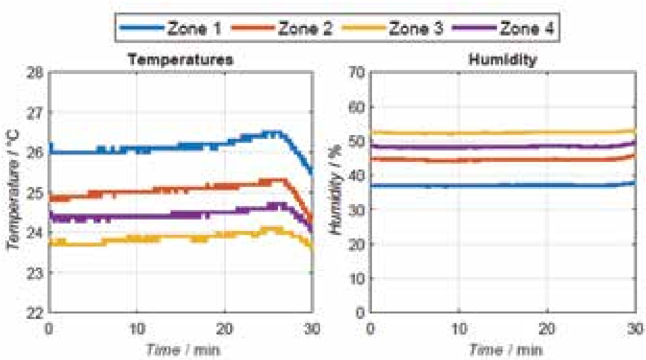

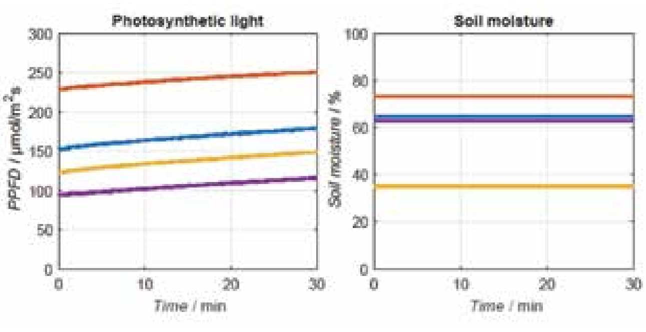

Fig. 2. Microclimate in 4 zones for an exemplary case study.

of temperature, humidity, light intensity, and soil moisture during a chosen period of 30 minutes.

Measured identifiers

Physiological identifiers such as stomatal transpiration, photosynthetic effect, night respiration, intercellular carbon dioxide concentration, evaporation, etc. are associated indirectly with physical and more accessible, measurable vegetation indices relying mostly on multi-spectral cameras as sensors. This is necessary to enable a large number of measurements, as accurate plant status identifiers from the domain of molecular biology are both time-consuming and costly, and may be associated with a correlation delay with respect to other input-output data. In order to capture both the spectral bands required for basic vegetation indices as well as additional bands to power further analytics, a multi-spectral sensor RedEdge-MX was chosen.

4. Software architecture

The architecture of the chamber's software support (depicted in Fig. 3) includes the established i) database on the central data server, ii) computer cloud architecture, directly connected with iii) sensors and actuators of the devices utilised to conduct experiments. The data from the sensors and actuators are collected every 15 minutes and stored in the cloud computer; from there they are retrieved once a day, stored in the central server database and made available for advanced analysis.

Device software layer: divided into multiple subsystems, namely the control and regulation subsystem, the network subsystem and multiple sensor subsystems. The embedded controller in the control and regulation subsystem is a real-time controller for ensuring desired environmental conditions within the devices, i.e. wired connectivity with the sensors and actuators, and real-time execution of the control loops. The architecture of the device's software, along with actuator and sensor control, implies the established communication with the computer cloud through which telemetry data and status reports are sent.

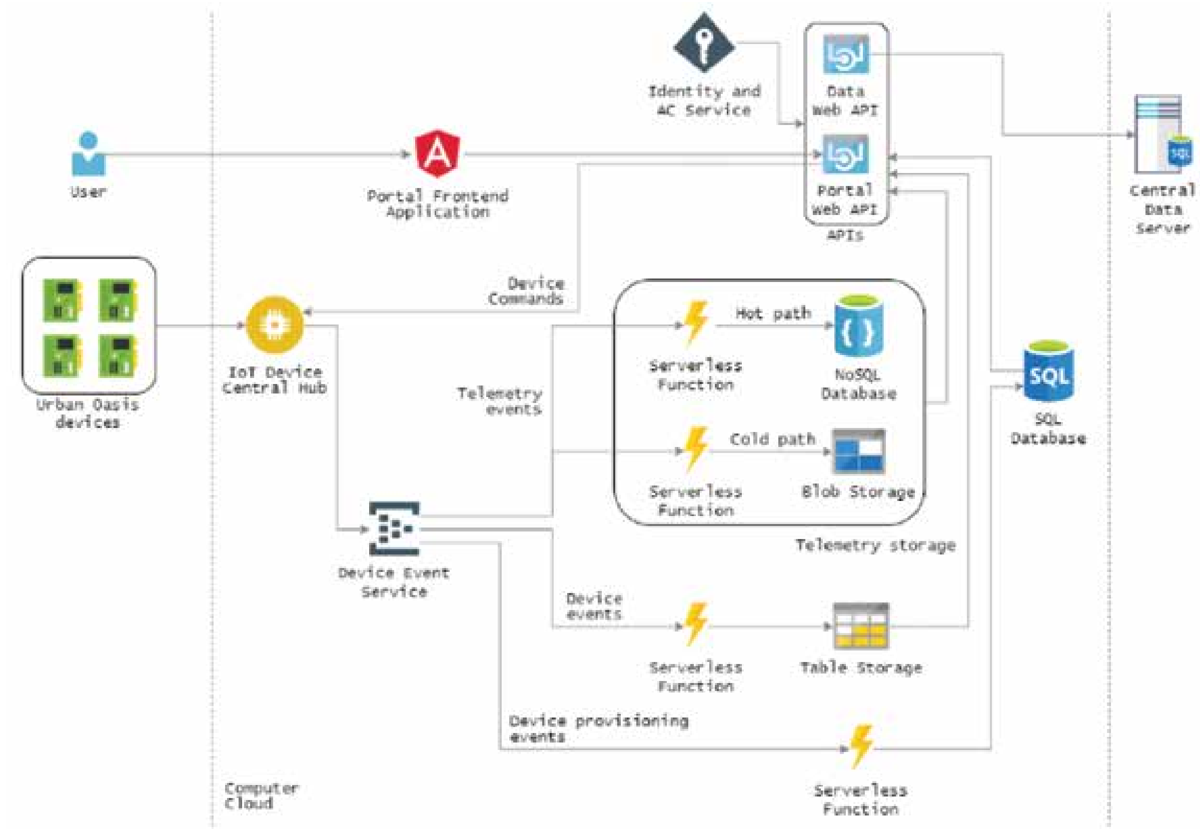

Fig. 3. Schematic of the IT system for collection and storage of the encapsulated design measured data.

Computer cloud layer: designed for three main functions: i) telemetry ingestion and analysis, ii) device maintenance and control and iii) presentation of aggregated data and analysis results. Individual devices are connected to the cloud services through a central node where the device telemetry and status messages are aggregated and routed to distinct endpoints.

Central data server: a local server that collects the telemetry data and status reports from multiple encapsulated design devices, archives the data and conducts the advanced data processing such as experiments scheduling or executing tailored AI algorithms. The server integrates the data from all the growing chambers and makes it available for advanced processing, i.e. modelling through the use of ML approaches. Along the data collected from the chambers via the cloud service, pictures obtained from the multi-spectral cameras are also stored on the central server computer, thus rounding up the available data from the plant development side.

5. Modeling of crop growth stages

With a significant amount of relevant data made available through the plant growth encapsulated design and the corresponding IT system, AI techniques, i.e. ML algorithms are employed to correlate the measured climate conditions with plant development indicators. In addition to the microclimate conditions and plant physiological identifiers data entries, short- and long-term weather forecasts are included in the dataset. The weather forecasts are provided by the Croatian Meteorological and Hydrological Service.

In accordance with the usual ML practice, the available dataset is divided into train, validation and test counterparts. Additionally, to significantly increase the reliability of prediction, models are classified and reduced to three parts, depending on the plant stage: i) germination, ii) plant formation and maturation, iii) grain maturation, and training is conducted on such divided data sets.

Several separate modules are developed based on the plant development indicators used as modelled outputs:

- yield prediction module,
- module for grain moisture prediction in current conditions and short-term prognosis,
- module for support in optimal pest treatment,
- module for long-term prediction of culture in climate change.

Once developed and tuned, the models will be publicly and interactively used through a web-based portal for predicting plant development under real and hypothetical climate conditions, with accumulated and archived feedback from farmers as additional data to tune the developed models.

Models of all three plant stage developments can be combined in order to offer insight into the overall plant development when new climate conditions are introduced. This option offers the possibility to simulate the wheat culture development in new environments that are likely to occur due to the climate changes already in effect. Such information can help in the determination of more fertile wheat cultivars and provide a general insight into crop development in the near future.

6. Conclusion

A system of encapsulated design devices for permutation of microclimate conditions and plant development monitoring is being elaborated. The system incorporates the concept of Internet of Things with real-time control and interfaces, and communication with a computer cloud that enable autonomous conduction of a large number of simultaneous experiments in microclimate zones of the device. It is used to rapidly gather a large amount of correlated data, thus enabling the artificial intelligence modelling of wheat development with respect to expected climate changes, i.e. predictive agriculture.

References

[1.] L. Chettri and R. Bera, "A comprehensive survey on internet of things (IoT) toward 5G wireless systems," IEEE Internet of Things Journal, vol. 7, no. 1, pp. 16–32, 2020.

[2] M. S. Farooq, S. Riaz, A. Abid, K. Abid, and M. A. Naeem, "A survey on the role of IoT in agriculture for the implementation of smart farming," IEEE Access, vol. 7, pp. 156 237–156 271, 2019.

[3] O. Elijah, T. A. Rahman, I. Orikumhi, C. Y. Leow, and M. N. Hindia," An Overview of Internet of Things (IoT) and Data Analytics in Agriculture: Benefits and Challenges," IEEE Internet of Things Journal, vol. 5, no. 5, pp. 3758–3773, 2018.

[4] K. Jha, A. Doshi, P. Patel, and M. Shah, "A comprehensive review on automation in agriculture using artificial intelligence," Artificial Intelligence in Agriculture, vol. 2, pp. 1–12, 2019.

[5] M. Roopaei, P. Rad, and K. Choo, "Cloud of things in smart agriculture: Intelligent irrigation monitoring by thermal imaging," IEEE Cloud Computing, vol. 4, no. 1, pp. 10–15, 2017.

[6] K. G. Liakos, P. Busato, D. Moshou, S. Pearson, and D. Bochtis," Machine learning in agriculture: A review," Sensors, vol. 18, no. 8,2018.

[7] R. K. Singh and Prajneshu, "Artificial Neural Network Methodology for Modelling and Forecasting Maize Crop

Yield," Agricultural Economics Research Review, vol. 21, no. 1, 2008.

[8] S. Wolfert, L. Ge, C. Verdouw, and M.-J. Bogaardt, "Big data in smartfarming – a review," Agricultural Systems, vol. 153, pp. 69–80, 2017.

[9] J. C. Zadoks, T. T. Chang, and C. F. Konzak, "A decimal code for the growth stages of cereals," Weed Research, vol. 14, no. 6, pp. 415–421,1974.

[10] S. Chandra, H. Lata, I. A. Khan, and M. A. Elsohly, "Photosynthetic response of cannabis sativa l. to variations in photosynthetic photon flux densities, temperature and CO_2 conditions," Physiology and Molecular Biology of Plants, vol. 14, no. 4, pp. 299–306, 2008.

[11] V Lešić, H. Novak, M. Ratković, M. Zovko, D. Lemić, S. Skendžić, J. Tabak, M. Polić, and M. Orsag, "Rapid Plant Development Modelling System for Predictive Agriculture Based on Artificial Intelligence", 16th International Conference on Telecommunications - ConTEL, pp. 173–180, 2021

Vol. 16(3) 2021 – ISSN 1331-7210

Engineering Power – *Bulletin of the Croatian Academy of Engineering*

Publisher: Croatian Academy of Engineering (HATZ), 28 Kačić Street, P.O. Box 14, HR-10001 Zagreb, Republic of Croatia

Editor-in-Chief: Prof. Vladimir Andročec, Ph.D., President of the Academy retired Full Professor with tenure, University of Zagreb, Faculty of Civil Engineering

Editor: Prof. Zdravko Terze, Ph.D., Vice-President of the Academy University of Zagreb, Faculty of Mechanical Engineering and Naval Architecture

Guest-Editor: Professor Emeritus Nedjeljko Perić – Innovation centre Nikola Tesla, and University of Zagreb, Faculty of Electrical Engineering and Computing

Editorial Board: Prof. Vladimir Andročec, Ph.D., Prof. Zdravko Terze, Ph.D., Prof. Vladimir Mrša, Ph.D.

Editorial Board Address: Croatian Academy of Engineering (HATZ), "Engineering Power" – Bulletin of the Croatian Academy of Engineering, Editorial Board, 28 Kačić Street, P.O. Box 14, HR-10001 Zagreb, Republic of Croatia

E-mail: hatz@hatz.hr

Graphical and Technical Editor: Minerva Graphica, Ltd., Zagreb

Proof-reader: Miroslav Horvatić, MA

Press: Tiskara Zelina, Ltd., Zelina

Circulation: 200